Mitochondrial Phosphopantetheinylation is Required for Oxidative Function

Pieter R. Norden[1, *], Riley J. Wedan[1,2, *], Samuel E. J. Preston[1], Morgan Canfield[1], Naomi Graber[1], Jacob Z. Longenecker[1], Olivia A. Pentecost[1], Elizabeth McLaughlin[1], Madeleine L. Hart[1], and Sara M. Nowinski[1]

[1]Department of Metabolism and Nutritional Programming, Van Andel Institute, Grand Rapids, MI

[2]College of Human Medicine, Michigan State University, Grand Rapids, MI

*These authors contributed equally

Correspondence:

Sara.nowinski@vai.org (S.N.)

Abstract

4'-phosphopantetheinyl (4'PP) groups are essential co-factors added to target proteins by phosphopantetheinyl transferase (PPTase) enzymes. Although mitochondrial 4'PP-modified proteins have been described for decades, a mitochondrially-localized PPTase has never been found in mammals. We discovered that the cytoplasmic PPTase aminoadipate semialdehyde dehydrogenase phosphopantetheinyl transferase (AASDHPPT) is required for mitochondrial respiration and oxidative metabolism. Loss of AASDHPPT results in failed 4'PP modification of the mitochondrial acyl carrier protein and blunted activity of the mitochondrial fatty acid synthesis (mtFAS) pathway. We found that in addition to its cytoplasmic localization, AASDHPPT localizes to the mitochondrial matrix via an N-terminal mitochondrial targeting sequence contained within the first 20 amino acids of the protein. Our data show that this novel mitochondrial localization of AASDHPPT is required to support mtFAS activity and oxidative function. We further identify five variants of uncertain significance in *AASDHPPT* that are likely pathogenic in humans due to loss of mtFAS activity.

Keywords:

Mitochondria, fatty acid synthesis, electron transport chain, reductive carboxylation, metabolism, respiration, compartmentalization, phosphopantetheine

35 Abbreviations:
36 4'PP – 4'-phosphopantetheine/yl,
37 AASDHPPT – aminoadipate semialdehyde dehydrogenase phosphopantetheinyl
38 transferase,
39 ALDH1L2 – Aldehyde Dehydrogenase 1 Family Member L2,
40 ATP5a – ATP synthase F1 subunit alpha,
41 BiFC – bimolecular fluorescence complementation,
42 CoA – coenzyme A,
43 CS – citrate synthase,
44 DHRS2 – mitochondrial Dehydrogenase/Reductase 2,
45 DLAT – dihydrolipoyllysine-residue acetyltransferase,
46 DLST – dihydrolipoamide S-succinyltransferase,
47 ETC – electron transport chain,
48 FAS – fatty acid synthesis,
49 FASN – fatty acid synthase,
50 FeS – iron sulfur cluster,
51 LA – lipoic acid,
52 LCMS – liquid chromatography mass spectrometry,
53 LYRM – leucine tyrosine arginine motif,
54 mtFAS – mitochondrial fatty acid synthesis,
55 MFN2 – mitofusin 2,
56 MTS – mitochondrial targeting sequence,
57 NAD^+ – nicotinamide adenine dinucleotide (oxidized form),
58 NDUFAB1 – NADH:ubiquinone oxidoreductase subunit AB1,
59 OGDH – oxoglutarate dehydrogenase,
60 PAGE – polyacrylamide gel electrophoresis,
61 PDH – pyruvate dehydrogenase,
62 PMS – post-mitochondrial supernatant,
63 PPT – mammalian AASDHPPT, PPTase – phosphopantetheinyl transferase,
64 PTM – posttranslational modification,
65 SDHB – succinate dehydrogenase subunit B,
66 TCA – tricarboxylic acid,
67 VC – venus c' terminus,
68 VN – venus n' terminus,

69 VUS – variant of uncertain significance

70

71 **Main**

72 4'-phosphopantentheinylation is an essential post translational modification (PTM)
73 whereby a 4'-phosphopantetheine (4'PP) group, derived from coenzyme A (CoA), is covalently
74 attached to target proteins by a phosphopantetheinyltransferase (PPTase) enzyme[1]. A total of
75 six proteins in the mammalian proteome have been found to have a 4'PP-modified serine:
76 three cytoplasmic proteins (Fatty Acid Synthase, FASN; Aminoadipate semialdehyde
77 dehydrogenase, AASDH; and Aldehyde Dehydrogenase 1 Family Member L1, ALDH1L1),
78 and three mitochondrial proteins (NADH:Ubiquinone Oxidoreductase Subunit AB1,
79 NDUFAB1; Aldehyde Dehydrogenase 1 Family Member L2, ALDH1L2; and mitochondrial
80 Dehydrogenase/Reductase 2, DHRS2)[1]. In mammalian genomes, only one PPTase has been
81 annotated—aminoadipate-semialdehyde dehydrogenase- phosphopantetheinyl transferase
82 (AASDHPPT)—which was thought to exist solely in the cytoplasm[2]. This contrasts with other
83 species such as *Arabidopsis thaliana* and *Saccharomyces cerevisiae,* which have dedicated
84 mitochondrial PPTases, the activity of which cannot be compensated by cytoplasmic PPTase
85 proteins[3,4]. It was therefore unclear how 4'PP is attached to mitochondrial proteins in
86 mammalian cells.

87 Since no mammalian mitochondrial PPTase had ever been described, we questioned
88 whether an unidentified PPTase existed in mammals, or conversely if AASDHPPT (hereafter
89 abbreviated PPT) was important for mitochondrial function regardless of its reported
90 cytoplasmic localization. One prior study found that PPT could add a 4'PP group to purified
91 mitochondrial proteins *in vitro*, but concluded that its activity was greater than 90%
92 cytoplasmic, raising questions as to whether this activity was biologically relevant[2]. We
93 therefore set out to understand whether PPT is required for mitochondrial function and, if so,
94 how it modifies mitochondrial targets despite existing in separate cellular compartments.

95 To test whether PPT is required for mitochondrial oxidative function, we used a
96 CRISPR/Cas-9-based strategy to mutate *Aasdhppt* in C2C12 mouse skeletal muscle
97 myoblasts. Complete loss of PPT was incompatible with growth; however, we generated two
98 clonal cell lines with hypomorphic mutations in *Aasdhppt* (Extended Data Fig. 1A) that resulted
99 in decreased PPT protein levels (PPT-1 and PPT-2, Fig. 1A). These results were confirmed
100 by siRNA-mediated knockdown of the same target (siPPT-1 and siPPT-2, Fig. 1A). Of note,
101 C2C12 cells have been shown to be near-tetraploid[5,6]. Consequently, we found three alleles
102 with unique PPT gene sequences in each of our PPT-deficient C2C12 cell lines (Extended

103 Data Fig. 1A). In both cases, the top listed allele in Extended Data Fig. 1A was found about
104 twice as frequently as the other two sequences in each cell line, likely indicating that there are
105 two alleles with this sequence. Further, our sequencing analysis revealed that the PPT-2 cells
106 still harbor at least one wild type allele, which corresponded to a low level of residual wild type
107 PPT protein expression, also visible by western blot (Fig. 1A and Extended Data Fig. 1A).
108 PPT-2 thus often displays a milder phenotype when compared directly with PPT-1, even
109 though both exhibit a loss of PPT protein abundance (Fig. 1A).

110 We next asked whether PPT deficiency resulted in altered respiratory-dependent growth
111 by culturing cells in media with either glucose or galactose, the latter requiring functional
112 mitochondrial respiration. Both PPT-deficient cell lines showed significantly increased
113 doubling times in both glucose-and galactose-containing media, which was rescued by
114 transient re-expression of full length PPT with a C-terminal GFP-Flag tag (PPT-GFP) (Fig. 1B-
115 C, Extended Data Fig. 1B-C). Next, we performed a Seahorse mitochondrial stress test and
116 observed that PPT-deficient mutants exhibited a reduction in both basal respiration rate and
117 maximal respiration rate compared to controls, rescued by re-expression of wild type PPT-
118 GFP (Fig. 1D, Extended Data Fig. 1D). To assess whether PPT-deficient respiratory function
119 was associated with perturbed OXPHOS complex expression and assembly, we performed
120 blue-native PAGE on isolated mitochondria from PPT-deficient and control cells. PPT-deficient
121 mutants displayed reduced levels of fully assembled electron transport chain (ETC) complex
122 I (CI), complex II (CII) and complex IV (CIV). ATP synthase (CV) and complex III (CIII) were
123 not affected by PPT-deficiency, but reductions in CIII-containing supercomplexes (SC) were
124 observed. Lastly, assemblies of CI, II and IV were rescued by re-expression of wild type PPT-
125 GFP (Fig. 1E, Extended Data Fig. 1E). Together, these data demonstrate that PPT deficiency
126 results in dysfunctional mitochondrial respiratory and ETC-deficient phenotypes.

127 ETC impairments such as complex I dysfunction are well known to affect mitochondrial
128 metabolism and alter tricarboxylic acid (TCA) cycle flux and nutrient utilization[7–9]. Since PPT-
129 deficient cells display reduced levels of ETC complexes, we reasoned that they may also
130 display altered TCA metabolism. To assess TCA cycle activity, we cultured cells in fully labeled
131 ^{13}C-glutamine (U-[^{13}C]-Glutamine) for up to 6 hours and evaluated TCA cycle intermediates
132 for relative abundance and carbon contribution from U-[^{13}C]-labeled glutamine. This approach
133 allowed us to assess reductive (light gray) versus oxidative (dark gray) metabolism of
134 glutamine (Fig. 1F) both at steady state and over time. At steady state, PPT-deficient cells
135 demonstrated an increase in the pool size of succinate and a decrease in downstream
136 metabolites such as fumarate, malate, and aspartate (Fig. 1G, Extended Data Fig. 1F-H).

137 Citrate and α-ketoglutarate levels were variable (Extended Data Fig. 1I and J); however, the
138 ratio of malate abundance to citrate abundance was consistently reduced in PPT mutants
139 compared to controls (Fig. 1H). The reduction of TCA metabolites downstream of succinate
140 relative to citrate suggests decreased oxidative TCA processing in PPT-deficient cells.

141 To assess whether this was indeed the case, we examined citrate labeling patterns from
142 uniformly labeled glutamine. In general, M+4 citrate results from the oxidation of glutamine to
143 oxaloacetate, whereas M+5 citrate results from the reductive carboxylation of glutamine to
144 citrate. Increased reductive carboxylation is a common feature of respiratory-deficient cells[7,8],
145 because it affords cells an alternative pathway to regenerate NAD^+. In agreement with our
146 pool size data, which suggested a reduction in oxidative TCA processing, PPT-deficient cells
147 showed reduced M+4 citrate and increased M+5 citrate compared to controls, indicating
148 reduced oxidative TCA processing and increased reductive carboxylation of glutamine
149 (Extended Data Fig. 1K). This is further supported by the increase in the ratio of citrate
150 M+5:citrate M+4 at isotopic steady state (Fig. 1I). Accordingly, we also observe a decrease in
151 downstream M+4 malate (Extended Data Fig. 1L), likely due to a reduction M+4 citrate. In
152 sum, the glutamine labeling patterns in PPT-deficient cells demonstrate increased reductive
153 carboxylation of glutamine, which is typical of cells with ETC impairments[5]. Collectively, our
154 data show that PPT mutant cells exhibit loss of oxidative mitochondrial metabolism.

155 We next asked which mitochondrial target(s) of PPT were most prominently responsible
156 for the loss of mitochondrial oxidative function. As mentioned above, there are three known
157 4'PP-modified proteins in mammalian mitochondria, NDUFAB1, ALDH1L2, and DHRS2[1]. To
158 explore which of these putative targets displayed the strongest genetic relationships to PPT,
159 we analyzed gene co-dependency relationships from the DepMap Public 23Q4+ Score
160 Chronos dataset[10] to identify gene functionality within the same biological pathway[11]. Among
161 the three known mitochondrial 4'PP-modified proteins, *AASDHPPT* (PPT) gene effect was
162 positively correlated only with *NDUFAB1* (Pearson r = 0.24) (Extended Data Fig. 2A).

163 Unique among 4'PP-modified proteins, NDUFAB1 is a structural subunit of complex I of
164 the ETC, as well as an integral part of the mitochondrial fatty acid synthesis (mtFAS) pathway.
165 mtFAS builds *de novo* fatty acyl chains on NDUFAB1, which are required both as precursors
166 for the biosynthesis of lipoic acid (LA), an important TCA cycle enzyme co-factor, as well as
167 to stabilize ETC assembly factors and iron-sulfur (FeS) cluster biogenesis complexes via
168 protein-protein interactions with NDUFAB1[12,9]. Because the newly synthesized fatty acids are
169 added to the terminal sulfhydryl group of the 4'PP PTM, the addition of a 4'PP to NDUFAB1
170 is required for mtFAS to occur and to support these downstream pathways[13]. Of note, the

171 mtFAS pathway gene *OXSM* ranked third overall for co-dependency with *AASDHPPT*
172 (Pearson r = 0.42)[14] out of all genes in the Depmap database (Extended Data Fig. 2B).
173 Additional mtFAS pathway genes also ranked highly in terms of *AASDHPPT* co-dependency,
174 including *MCAT* and *MECR* (Pearson r = 0.36 and 0.32 respectively) (Extended Data Fig. 2C
175 and D). Given that the 4'PP modification is necessary for acyl synthesis on NDUFAB1, these
176 data suggest that impaired mitochondrial respiration, reduced levels of ETC complexes, and
177 altered TCA cycle metabolism in PPT-deficient cells may be a downstream result of diminished
178 mtFAS function, in agreement with the known roles of mtFAS[9,15].
179 To further explore the genetic relationships between *AASDHPPT* and mtFAS, we
180 performed clustering and two-dimensional mapping of pairwise gene essentiality score
181 correlations with *AASDHPPT*. We included genes associated with the GO term "pantothenate
182 metabolism" from the DepMap project database as well as all genes encoding known
183 phosphopantetheinylated proteins, mtFAS pathway genes, and genes involved in downstream
184 lipoic acid synthesis and ETC assembly - such as the leucine, tyrosine, arginine motif (LYRM)
185 assembly factors which are regulated by mtFAS[9]. The analyzed genes grouped into four
186 distinct clusters based on gene essentiality (Extended Data Fig. 2E). Two-dimensional
187 mapping of correlation distance showed that *AASDHPPT* most strongly correlated with mtFAS
188 pathway genes, as well as several LYRM family members, further suggesting that PPT may
189 act as a critical regulator of mtFAS functional activity (Fig. 2A).
190 To test this hypothesis, we examined whether PPT-deficiency altered known mtFAS
191 pathway endpoints, including protein lipoylation and succinate dehydrogenase subunit B
192 (SDHB) stability, which is a reliable surrogate of the LYRM-dependent ETC assembly
193 mechanism we previously described[9]. PPT-deficient cells exhibited reduced lipoylation of
194 pyruvate dehydrogenase (PDH) and α-ketoglutarate dehydrogenase (OGDH) subunits (DLAT
195 and DLST, respectively) along with reduced stability of SDHB (Fig. 2B), resembling the
196 molecular phenotype of mtFAS-deficient cells. These findings also agree well with our
197 metabolic tracing data, which suggest reduced TCA cycle activity downstream of SDH (Fig.
198 1H, Extended Data Fig.1F-H). PDH and OGDH lipoylation and SDHB stability were all rescued
199 by transient re-expression of PPT-GFP compared to a control vector expressing
200 mitochondrially localized DSRed (mtDSRed) (Fig. 2B).
201 Although one prior study demonstrated that PPT is able to add a 4'PP group to NDUFAB1
202 *in vitro*[2], its requirement for NDUFAB1 phosphopantetheinylation had never been tested in
203 mammalian cells. We noted that NDUFAB1 migrated faster on SDS-PAGE gels in PPT-
204 deficient cell lysates (Fig. 2B, Extended Data Fig. 2G), and hypothesized that this difference

205 in migration might correspond to loss of the 4'PP-modification, as unmodified apo-NDUFAB1
206 has previously been shown to migrate faster than 4'PP-modified holo-NDUFAB1 due to its
207 lower molecular weight[2]. We asked whether this downward shift in NDUFAB1 migration
208 corresponded to the 4'PP modification by mutating the modified serine to an alanine residue
209 (S112A), thereby blocking phosphopantetheinylation of NDUFAB1. We expressed wild type
210 NDUFAB1-Flag or NDUFAB1$_{S112A}$-Flag in both control and PPT-deficient cells and found that
211 NDUFAB1$_{S112A}$-Flag in control cells migrates at the same molecular weight as NDUFAB1-Flag
212 in PPT-deficient cells (Fig. 2C). Moreover, NDUFAB1$_{S112A}$-Flag does not display any further
213 downward shift in PPT-deficient cells, indicating that the two perturbations are not additive,
214 and are both likely to be due to loss of 4'PP at S112 (Fig. 2C).

215 To directly assess whether phosphopantetheinylation of NDUFAB1 is decreased in PPT-
216 deficient cells, we developed a method to detect 4'PP-modification of NDUFAB1 by liquid
217 chromatography mass spectrometry (LCMS), borrowing from an assay developed in plant
218 mitochondria and recently demonstrated for the first time in mammalian cell lines (Fig. 2D)[16,17].
219 We expressed and immunoprecipitated NDUFAB1-Flag in control and PPT-deficient cells and
220 found that our isolated NDUFAB1 exhibited a similar gel shift as we had observed by blotting
221 in whole cell lysates (Fig. 2E). We then digested these samples with an aspartate
222 endoproteinase (AspN), resulting in a tripeptide (Asp-Ser-Leu) that we could monitor for 4'PP-
223 or 4'PP-acyl modifications via LCMS. This allowed us to detect and quantify levels of apo-,
224 holo-, and octanoyl-NDUFAB1 from control and PPT-deficient cells, verified by standards
225 synthesized *in vitro* (Extended Data Fig. 2H). We found that relative to control cells, PPT-
226 deficient cells have reduced levels of both holo- and octanoyl-NDUFAB1 (Fig. 2F and G). The
227 PPT-1 clone displayed a striking accumulation of apo-NDUFAB1, in agreement with its
228 stronger loss of function phenotype. In addition to the loss of holo-NDUFAB1, we found a
229 modest increase in the levels of intracellular CoA in the PPT-1 and PPT-2 cell lines (Extended
230 Data Fig. 2F). From these data, we conclude that PPT is required for 4'PP modification of
231 NDUFAB1 and downstream mtFAS activity, including protein lipoylation, ETC assembly, and
232 mitochondrial respiration, which all require mtFAS products[15].

233 The question then became: if PPT is required for modification of mitochondrial proteins,
234 does it act in the cytoplasm, prior to mitochondrial import, or is there an undescribed
235 mitochondrial pool of PPT? To address this question, we performed immunofluorescence
236 staining for endogenous PPT and mitochondrial ATP synthase subunit 5a (ATP5a) and
237 assessed co-localization (Fig. 3A and B, Extended Data Fig. 3A-C). As expected, PPT
238 expression was significantly reduced in PPT-deficient cells compared to controls (Extended

239 Data Fig. 3B) and exhibited a punctate, perinuclear expression pattern that co-localized with
240 ATP5a staining in control cells (Pearson r = 0.60 and 0.62) (Fig. 3B). Additionally, signal in the
241 PPT channel was surprisingly observed in the nuclei of some cells (Fig. 3A, Extended Data
242 Fig. 3A).

243 To test whether this staining pattern was specific, we employed siRNA and found a similar
244 reduction in endogenous PPT signal as observed in our PPT-deficient cell lines, although
245 nuclear signal in the PPT channel was maintained despite knockdown (Extended Data Fig.
246 3D). We therefore also expressed PPT-Flag and performed immunofluorescent staining for
247 the Flag epitope and found a similar punctate, peri-nuclear staining pattern that overlapped
248 with citrate synthase staining but displayed no clear nuclear signal (Extended Data Fig. 3E).
249 These results indicate that a sub-population of PPT localizes specifically to mitochondria but
250 not to the nucleus.

251 We further verified the observed mitochondrial localization using subcellular fractionation
252 and Western blotting in control and PPT-deficient cells. We detected endogenous PPT
253 expression in both mitochondria and post-mitochondrial supernatant (PMS) (Fig. 3C). PPT
254 expression was reduced in both fractions, and nearly absent from mitochondria in PPT-
255 deficient cells (Fig. 3C). We also characterized subcellular localization of PPT-GFP using
256 immunofluorescence and found strong signal overlap with ATP5a (Fig. 3D), in agreement with
257 our prior observations.

258 We then asked whether this pool of mitochondrially-localized PPT was mitochondrially
259 associated or in the mitochondrial matrix with NDUFAB1 and the rest of the mtFAS machinery.
260 To tackle this question, we employed a bimolecular fluorescence complementation (BiFC)
261 system[18] to visualize the sub-mitochondrial localization of PPT. We used a split-Venus tag
262 technique in which the N-terminus of the Venus fluorophore (VN, residues 1-172) was
263 attached to either the N- or C-terminus of PPT, while the C-terminus of Venus (VC, residues
264 155-238) was attached to the C-terminus of a control protein with known localization. This
265 system allows us to observe fluorescent signal only when both halves of the split-Venus tag
266 are able to associate within a compartment[18]. For these control proteins, we chose Mitofusin
267 2 (MFN2) – a transmembrane protein that localizes on the outer mitochondrial membrane with
268 both its N- and C-termini facing the cytoplasm – along with citrate synthase (CS) and
269 NDUFAB1, both of which are matrix-localized. We quantified Venus fluorescence in each of
270 our BiFC conditions by flow cytometry, and observed significant Venus signal only when PPT-
271 VN cells were co-expressed with either CS-VC or NDUFAB1-VC, indicating that PPT localizes
272 to the mitochondrial matrix (Fig. 3E-G, see Extended data Fig. 3F for gating strategy).

273 Most mitochondrial proteins are encoded by nuclear genes and imported into mitochondria
274 via an N-terminal mitochondrial targeting sequence (MTS), consisting of approximately 20 to
275 40 amino acid residues[19]. Surprisingly, in cells expressing N-terminally tagged PPT (VN-PPT),
276 positive Venus fluorescence was only detected when co-expressed with MFN2-VC (Fig. 3E-
277 G), indicating that N-terminally tagged VN-PPT is mitochondrially associated on the OMM.
278 Since our BiFC data showed that tagging PPT on the N-terminus prevented its localization in
279 the mitochondrial matrix (Fig. 3E-G), we hypothesized that mitochondrial localization of PPT
280 may be driven by an N-terminal MTS.
281 To explore this hypothesis, we first analyzed the AASDHPPT coding sequence using the
282 MitoFates[20] and DeepMito[21,22] prediction algorithms. MitoFates reports a 41.5% probability of
283 a mitochondrial presequence at the N-terminus of AASDHPPT, with a TOM20 recognition
284 motif from amino acids 5-9 and an MPP cleavage site at amino acid 19 (W) (Fig. 4A and B).
285 Alternatively, DeepMito predicts a 47% probability of mitochondrial localization. This region of
286 the amino acid sequence is well conserved among mammals (Extended Data Fig. 4A). To test
287 whether the N-terminus of PPT is a bonafide MTS, we generated N-terminal truncations to
288 the next two methionine residues at positions 14 and 37 ($PPT_{\Delta 1\text{-}13}$-GFP and $PPT_{\Delta 1\text{-}36}$-GFP,
289 respectively, Fig. 4A) and examined their localization using fluorescence microscopy. While
290 PPT-GFP co-localized strongly with ATP5a, $PPT_{\Delta 1\text{-}13}$-GFP exhibited diffuse localization
291 throughout the nucleus and cytoplasm (Fig. 4C-D). $PPT_{\Delta 1\text{-}36}$-GFP exhibited weak fluorescent
292 expression mostly within the nucleus, suggesting that this larger N-terminal truncation
293 destabilizes PPT (Fig. 4C-D). To further refine the MTS based on the MitoFates prediction, we
294 also tested an N-terminal truncation replacing the first 20 amino acids with a single methionine
295 ($PPT_{\Delta 1\text{-}20}$-GFP). $PPT_{\Delta 1\text{-}20}$-GFP behaved similarly to $PPT_{\Delta 1\text{-}36}$-GFP, with very low levels of
296 diffuse expression (Extended Data Fig. 4B), perhaps indicative of instability upon completely
297 failed import. Sub-cellular fractionation and Western blotting supported our microscopy
298 results, showing that while PPT-GFP and $PPT_{\Delta 1\text{-}13}$-GFP are both present in PMS and
299 mitochondrial fractions, $PPT_{\Delta 1\text{-}13}$-GFP accumulates in the PMS (Fig. 4E), suggesting difficulty
300 in localizing to mitochondria.
301 We also performed the converse experiment, in which we added only the first 36 amino
302 acids of PPT to GFP, to test the sufficiency of the putative MTS to drive GFP to the
303 mitochondria (PPT MTS-GFP). PPT MTS-GFP showed strong overlap with ATP5a staining by
304 fluorescence microscopy as well as strong expression in the mitochondrial fraction via
305 Western blot (Extended Data Fig. 4C and D). We took a parallel BiFC approach using the
306 split-Venus tag system by expressing the first 36 amino acids of PPT fused to the N-terminus

307 of Venus (PPTaa$_{1-36}$-VN) with either MFN2-VC, CS-VC, or NDUFAB1-VC. As with C-terminally
308 tagged PPT-VN, significant Venus signal was only observed when PPTaa$_{1-36}$-VN was co-
309 expressed with either CS-VC or NDUFAB1-VC (Fig. 4F and G, see Extended Data Fig. 3F for
310 gating strategy), indicating that the first 36 amino acids of PPT are sufficient to target proteins
311 to the mitochondrial matrix.

312 To test whether this newfound mitochondrial localization is required for PPT to modify
313 mitochondrial target proteins, we transduced PPT-deficient cells with mtDSRed, PPT-GFP,
314 PPT$_{\Delta 1-13}$-GFP, or PPT$_{\Delta 1-36}$-GFP, and assessed mtFAS pathway activity. Expression of PPT-
315 GFP rescued protein lipoylation and SDHB stability, whereas PPT$_{\Delta 1-13}$-GFP and PPT$_{\Delta 1-36}$-GFP
316 both failed to rescue either of these mtFAS-dependent endpoints, nor did they rescue the gel
317 shift of NDUFAB1 (Fig. 5A, Extended Data Fig. 5A). These data demonstrate that
318 mitochondrial localization of PPT is required for 4'PP-modification of NDUFAB1. To further
319 investigate whether mitochondrial localization of PPT is required for ETC assembly and
320 OXPHOS activity, we performed BN-PAGE and Seahorse mitochondrial stress tests as before
321 with control and PPT-deficient cells expressing mtDSRed, PPT-GFP, or PPT$_{\Delta 1-13}$-GFP. We
322 found that ETC complex levels, along with basal and maximal oxygen consumption rates,
323 were rescued by expression of PPT-GFP, and that PPT$_{\Delta 1-13}$-GFP rescued less well than the
324 full length PPT-GFP construct (Fig. 5B-D, Extended Data Fig. 5B-D).

325 Next, we took advantage of the *Saccharomyces cerevisiae* mitochondrial PPTase, yPpt2,
326 (which is known to specifically reside in the matrix) to test if 4'PP mitochondrial modifications
327 rescue the mtFAS-associated mitochondrial defects observed in PPT mutant cells. Indeed,
328 yPpt2-V5 localizes strongly to mitochondria (Extended Data Fig. 5E) and efficiently restores
329 protein lipoylation, SDHB levels, and NDUFAB1 migration in PPT-deficient cells (Fig. 5E).
330 Notably, yPpt2-V5 expression does not rescue protein lipoylation or SDHB in cells deficient
331 for the mtFAS enzyme MECR, indicating that this rescue is specific to loss of PPT and cannot
332 compensate for direct impairments to mtFAS itself (Fig. 5E, Extended data Fig. 5F). Together
333 with our truncation mutant analyses, these data demonstrate that mitochondrial localization of
334 PPT is necessary and sufficient for phosphopantetheinylation of NDUFAB1, mtFAS pathway
335 activity, ETC assembly and mitochondrial respiration.

336 We recently described a pathogenic variant in the mtFAS gene *MCAT* c.812T>C; p.T271I
337 (rs760294168; NM_173467.4)[23]. As our data demonstrate that perturbed *Aasdhppt*
338 expression results in similar phenotypes as mtFAS loss, we wondered whether there may be
339 patients with pathological variants in *AASDHPPT*. We searched the ClinVar database[24] and
340 identified several missense variants of uncertain significance (VUS) in *AASDHPPT* that were

341 associated with suspected inborn genetic disease. We selected six of these variants for
342 analysis: c.343C>T; p.P12S (NM_015423.3), c.140G>A; pR47H (NM_015423.3), c.214G>T;
343 pA72T (NM_015423.3), c.235T>G; pW79G (NM_015423.3), c.247C>T; pR83C
344 (NM_015423.3), and c.286A>G; pK96E (NM_015423.3).

345 We created each of these missense mutations in our full length PPT-GFP construct and
346 assessed their ability to rescue perturbed mtFAS activity in our PPT-deficient cells. We found
347 that all variants, with the exception of PPT-GFP P12S, exhibited weaker rescue effects than
348 wild type PPT (Fig. 5F, Extended Data Fig. 5G). These variants of PPT were also unable to
349 completely rescue basal, ATP-production coupled, or maximal respiration rates compared to
350 wild type PPT-GFP (Fig. 5G and H). Of note, cells expressing the PPT-GFP W79G variant
351 showed low levels of protein expression compared to the other variants (Fig. 5F, Extended
352 Data Fig. 5G-H) despite expression from the same promoter, suggesting that this variant may
353 result in protein instability. These data identify R47H, A72T, W79G, R83C, and K96E as
354 potential clinically observed pathologic variants of *AASDHPPT*, with molecular phenotypes
355 attributable to altered mtFAS activity and perturbed cellular respiration.

356 Our data position PPT as a critical mediator of mitochondrial oxidative function, due to its
357 requirement for proper function of the mtFAS pathway. While we show definitively that
358 mitochondrial PPT is required for phosphopantetheinylation of NDUFAB1, we did not explore
359 its involvement in 4'PP-modification of ALDH1L2 and DHRS2 in the present study. Future
360 work focused on the role of PPT in these additional pathways will be important to expand our
361 understanding of the full scope of PPT action in cells. The discovery of distinct pools of PPT
362 raises questions about what factors control PPT activity in each compartment. For instance,
363 PPT uses CoA as the substrate for 4'PP-modification of target proteins. How perturbations in
364 CoA availability affect PPT enzymatic activity may have important implications for PPT targets
365 such as mtFAS in diseases with CoA dysregulation[25]. Moreover, our data demonstrate that
366 PPT is targeted to mitochondria via an N-terminal MTS, but how this localization is controlled
367 in cells to produce two distinct pools is completely unstudied. Whether PPT localization is
368 dynamic will also be an interesting and important area for future study. Of note, we identified
369 five probable pathogenic patient variants in *AASDHPPT*. Our results predict that patients
370 harboring these mutant alleles likely exhibit impaired mtFAS, leading to diminished
371 mitochondrial function. These data add to the growing list of patients with pathogenic variants
372 in mtFAS and lipoic acid synthesis genes and support the notion that impairments in CoA
373 metabolism may cause disease via mtFAS dysfunction[26,27].
374

375 **Methods**

376

377 ***Aasdhppt mutant cell lines, siRNA transfection, growth assays, and viral transduction***
378 ***Cell Culture***

379 C2C12 immortalized mouse skeletal myoblasts (ATCC CRL-1772, verification provided by
380 ATCC) were grown in DMEM supplemented with 4.5 g/L glucose, glutamine, and sodium
381 pyruvate (Corning, 10-013-CV) and 10% FBS (Sigma, F0926) in humidified tissue culture
382 incubators (37°C, 5% CO_2).

383

384 **Generation of Aasdhppt mutant cell lines**

385 Four sgRNA sequences (**Table 1)** were designed targeting exon 1 or exon 2 of the mouse
386 *Aasdhppt* gene and subcloned into the pLentiCRISPR v2 vector using previously described
387 methods[28]. Parental C2C12s were transiently transfected with pLentiCRISPRv2_sgAasdhppt
388 or empty vector using a JetOptimus lipid transfection reagent (Polyplus, 76299-630). 48 hours
389 after transfection, cells were sorted on GFP signal intensity and plated into 96-well plates to
390 obtain single cell colonies for expansion and establishment of stable, clonal cell lines. Clones
391 were screened for AASDHPPT protein expression levels and two control clones and two
392 *Aasdhppt* mutant clones were selected for further experiments. While PPT-deficient clones
393 were derived from both guide RNAs, clones with the strongest loss of PPT expression were
394 all derived from sgRNA 1, and we focused further analyses on these clones with the strongest
395 loss of function phenotypes.

396

397 **Production of siRNA knockdown cell lines**

398 To knockdown *Aasdhppt* or *Ndufab1* expression, two Silencer Select pre-designed siRNAs
399 targeting *Aasdhppt* were acquired from Thermo Fisher Scientific and an ON-TARGETplus
400 SMARTpool siRNA targeting *Ndufab1* was acquired from Horizon Discovery (**Table 2**). The
401 siRNAs were packaged with Lipofectamine RNAiMAX transfection reagent for 30 minutes at
402 room temperature according to manufacturer instructions. C2C12 cells were transfected with
403 the siRNA mixture for a final concentration of 40 nM overnight. The following day, cells were
404 provided with fresh growth media and cells were cultured for 72 hours post-transfection to
405 either collect whole-cell lysates for western blot analysis or be fixed in 4% paraformaldehyde
406 for immunofluorescence analysis. C2C12 cells were transfected with ON-TARGETplus Non-
407 targeting Control Pool (D-001810-10-05) as a control.

408

409 **Retroviral backbone design**

410 For co-localization and rescue experiments, control and *Aasdhppt* mutant clonal lines
411 were transiently infected with retrovirus harboring a control transfer plasmid expressing
412 mtDSRed (pQXCIP mtDSRed) or pMMLV retrovirus vectors custom designed, synthesized,
413 and purchased from VectorBuilder (Chicago, IL, USA), harboring full length, or N-terminal
414 truncations of residues 1-13 or 1-36, of AASDHPPT with C-terminal GFP and Flag tag- fusion,
415 or yPPT2 with C-terminal Flag tag-fusion. *Site-directed mutagenesis.* For generation of
416 retrovirus constructs harboring single point mutations in the full length AASDHPPT-GFP-Flag
417 construct, primers in **Table 3** were used with a New England Biolabs Q5 Site-Directed
418 Mutagenesis Kit. Plasmid reactions were transformed into competent *E. coli* and selected
419 colonies were sequence validated for successful incorporation of point mutations.

420

421 **Growth Assays**

422 For growth assays 5,000 cells/well were plated in 24-well plates and grown in DMEM with
423 either 10% FBS, 4 mM glutamine, and 25 mM glucose for 4 days or 20% FBS, 4 mM
424 glutamine, and 10 mM galactose for 2 days in technical quadruplicates. Tissue culture plates
425 were placed in an IncuCyte® chamber (Sartorius) and percent confluency was measured from
426 sixteen images at 10X magnification per well every 3 hours. Percent confluency curves from
427 technical replicates were fit with a non-linear regression during the logarithmic growth phase
428 using the exponential growth equation in GraphPad Prism to determine population doubling
429 time.

430

431 ***Genomic Sequence Analysis of AASDHPPT Mutants***

432 Approximately five million cells of each clonal mutant cell line, PPT-1 and PPT-2, were
433 pelleted and washed with PBS then frozen at -80ºC. Genomic DNA was extracted using a
434 column-based kit assay (Qiagen 69504). Aasdhppt was amplified using primers described in
435 **Table 4**, and sanger sequenced using the forward primer. Sanger sequences were analyzed
436 using Snapgene software.

437

438 ***Crude mitochondrial isolation***

439 Cells were harvested and processed as previously described[9]. Briefly, cells were
440 harvested by trypsinization, washed once with cold, sterile PBS (Gibco, 10010-023), then
441 stored at -80°C. At the time of mitochondrial isolation, cell pellets were thawed and
442 resuspended in 1 mL CP-1 buffer (100 mM KCl, 50 mM Tris-HCL, 2 mM EGTA, pH 7.4)

443 supplemented with mammalian protease inhibitor cocktail (mPIC, Millipore Sigma P8340) and
444 mechanically lysed by 10 passes through a 1 mL insulin syringe with 26-guage needle and
445 centrifuged at 700 x g for 10 minutes to pellet unlysed cells and debris. Supernatant was
446 transferred to a new microcentrifuge tube and centrifuged at 10,000 x g for 10 minutes to
447 pellet the crude mitochondrial fraction. Post-mitochondrial supernatant (PMS) was used for
448 Western blot analysis or discarded. Mitochondrial pellets were resuspended in a small volume
449 of either RIPA buffer (10 mM Tris-HCl, pH 8.0, 1 mM EDTA, 0.5 mM EGTA, 1% Triton X-100,
450 0.1% Sodium Deoxycholate, 0.1% SDS, 140 mM NaCl) supplemented with mPIC, or CP-1
451 buffer, equal to approximately twice the pellet volume. Resuspended pellets were then used
452 for applications described below.
453
454 ***SDS-PAGE and immunoblotting***
455 Cultured cells were scraped from tissue culture plates directly into RIPA buffer
456 supplemented with mammalian protease inhibitor cocktail (mPIC, Millipore Sigma) and Pierce
457 Universal Nuclease, incubated at 4°C with constant agitation on a microcentrifuge tube orbital
458 shaker, then centrifuged at 17,000 x g for 20 minutes at 4°C to remove insoluble material.
459 Supernatant was then transferred to a new microcentrifuge tube to be saved as whole cell
460 lysate (WCL). For protein analysis, WCL, PMS, and/or crude mitochondrial fractions were first
461 normalized for total protein content via Pierce BCA Protein assay (Thermo Fisher Scientifc
462 23225). Samples were resolved by SDS-PAGE and transferred to nitrocellulose membranes.
463 Immunoblotting was performed using the indicated primary antibodies (**Table 5**) with
464 visualization and analysis of protein signal using Rabbit and Mouse IgG Antibody DyLight 680,
465 or 800, Conjugated secondary antibodies and Bio-Rad ChemiDoc Imaging System.
466 Alternatively, secondary anti-mouse or anti-rabbit HRP antibody and SuperSignal West Femto
467 Maximum Sensitivity Substrate (Thermo Fisher Scientific 34096) were used to visualize band
468 signals.
469
470 ***Seahorse Extracellular Flux Rate Assay***
471 Extracellular flux rate assays were performed on a Seahorse XFe96 Analyzer (Agilent).
472 Cells from the indicated clones and experimental conditions were plated in approximately 22
473 wells of a 96-well seahorse plate at a density of 8,000 (clonal controls) or 10,000 (PPT-
474 deficient clones) cells/well in DMEM +10% FBS and allowed to adhere overnight. The morning
475 of the assay, cells were washed twice and media was replaced with non-buffered seahorse
476 media (Agilent 103680) supplemented with 25mM glucose, 2mM glutamine, and 1mM sodium

477 pyruvate. A standard mitochondrial stress test was then performed using 1μM oligomycin,
478 3μM FCCP, and 0.5μM Rotenone + 0.5μM Antimycin A. Baseline oxygen consumption was
479 measured three times, followed by acute injection of oligomycin, followed by FCCP and finally
480 Rotenone + Antimycin A. Measurements were standard, with acute injection of drug followed
481 by 3 minutes of mixing then measurements of oxygen levels over 3 minutes, with three
482 measurements per phase. Data were normalized with crystal violet absorption for
483 approximation of cell number or by measurement of well % confluency using an IncuCyte®
484 chamber and a 10X magnification image field per well. Results were analyzed in WAVE
485 software and the Agilent Seahorse Analytics browser-based application for quantification of
486 basal, maximal, ATP-production coupled, and proton leak respiration.
487
488 ***Blue Native-PAGE***
489 Crude mitochondrial fractions were prepared and normalized for total protein content as
490 previously described. 100 μg of mitochondria were pelleted at 12,500 x g for 5 minutes at 4°C.
491 Supernatant was removed and pellets were resuspended in 54 μL of 1x pink lysis buffer
492 (Invitrogen BN2003). Digitonin (GoldBio D-180-2.5) was added to samples at a final
493 concentration of 1% mass/volume and samples were incubated on ice for 15 min. Insoluble
494 material was pelleted by centrifugation at 17,000 x g for 20 minutes and supernatant was
495 transferred to new microcentrifuge tubes. 3 μL of NativePAGE sample buffer (Invitrogen
496 BN2004) was added to samples and 10 μL of sample (~16 μg of crude mitochondrial fraction)
497 was loaded per lane on pre-cast 3-12%, Bis-Tris NativePAGE gels (Invitrogen BN1001BOX)
498 with NativePAGE anode buffer (Invitrogen 2001) and dark blue cathode buffer (Invitrogen
499 BN2002) at 150V for 30-40 minutes then switched to light blue cathode buffer and run at 20
500 V overnight. Gels were then transferred to PVDF membranes (pre-activated in 100%
501 methanol) at 100 V for 2 hours. Following transfer, membranes were washed in 8% acetic
502 acid solution for 5 minutes, washed in sterile distilled water twice for 5 minutes, then washed
503 in 100% methanol thrice for 5 minutes, and finally washed in sterile distilled water thrice for 5
504 minutes. Membranes were then blocked in 5% BSA solution at room temperature. Following
505 blocking, membranes were incubated with the indicated primary antibodies overnight at 4°C
506 (**Table 5)**. Secondary anti-mouse or anti-rabbit HRP antibody and SuperSignal West Femto
507 Maximum Sensitivity Substrate (Thermo Fisher Scientific 34096) was used to visualize bands
508 with a Bio-Rad ChemiDoc Imaging System.
509
510 ***Glutamine Tracing***

511 The indicated clonal cell lines were plated in 6-well plates in triplicate at a density of 200K
512 for PPT-1 and PPT-2, and 175K for Ctrl-1 and Ctrl-2 to account for differences in growth rate.
513 Cells were allowed to adhere for two hours, at which point the media was changed to
514 unlabeled media (Corning DMEM 17-207-CV with 1mM sodium pyruvate, 5mM glucose, and
515 4mM glutamine). After twenty hours in unlabeled media, wells were changed to labeled media
516 at the indicated time points prior to harvest (Corning DMEM 17-207-CV with 1mM sodium
517 pyruvate, 5mM glucose, and 4mM $U^{13}C$-glutamine). Three wells per cell line were left
518 unlabeled for natural isotope abundance correction, and another three per cell line were used
519 to determine cell number at the time of freezing. 24 hours after cells were in unlabeled media,
520 all wells were washed with normal saline once and frozen at -80°C. Plates were then extracted
521 for metabolites using a volume of 40:20:20 methanol:acetonitrile:water scaled to the number
522 of cells determined by the cell count wells (average from three wells). Lysates were sonicated
523 and incubated on ice for 60 minutes. At this point any insoluble material was spun out of the
524 sample at 17,000 x g for 10 minutes at 4°C. 1000 µL of supernatant was dried using a
525 SpeedVac concentrator.
526
527 ***Liquid chromatography – Mass Spectrometry***
528 Dried metabolomics extracts were next resuspended in 100% water containing 25 µg/mL
529 D5-Glutamate (DLM-556, Cambridge) such that resuspension sample equivalents were
530 5.82E+3 cells/µL. 2 µL of resuspended samples were injected on column, a process blank
531 was analyzed before and after experimental samples, and a pooled sample was injected twice
532 before experimental samples for column conditioning, and every 7-10 sample injections
533 thereafter. Data dependent MS2 (ddMS2) data was collected from pooled experimental
534 replicates to identify group-specific compounds.
535 Data were collected on a Vanquish liquid chromatography system coupled to an Orbitrap
536 Exploris 240 (Thermo Fisher Scientific) using a heated electrospray ionization (H-ESI) source
537 in ESI negative mode. All samples were run through a 24-minute reversed-phase
538 chromatography ZORBAX extend-C18 column (1.8µm, 2.1mm × 150mm, 759700-902,
539 Agilent, California, USA) combined with a guard column (1.8µm, 2.1mm × 5mm, 821725-907,
540 Agilent). Mobile phase A was LC/MS H2O (W6-4, Fisher) with 3% LC/MS grade methanol
541 (A456-4, Fisher), mobile phase B was LC/MS grade methanol (A456-4, Fisher), and both
542 mobile phases contained 10 mM tributylamine (90780-100ML, Sigma), 15 mM acetic acid,
543 and 0.01% medronic acid (v/v, 5191-4506, Agilent). For the re-equilibration gradient, mobile
544 phase A was kept the same, and mobile phase B was 99% LC/MS grade acetonitrile (A955-

545 4, Fisher). Column temperature was kept at 35ºC, flow rate 0.25 mL/min, and the solvent
546 gradient was as follows: 0-2.5 min held at 0% B, 2.5-7.5 min from 0% B to 20% B, 7.5-13 min
547 from 20% B to 45% B, 13-20 min from 45% B to 99% B, and 20-24 min held at 99% B. The
548 analytical solvent gradient was followed by a 16 min re-equilibration gradient to prep the
549 column before the next sample injection that went as follows: 0-0.05 min held at 99% B at
550 0.25 mL/min, 0.05-1 min from 99% B to 50% B and 0.25 mL/min to 0.1 mL/min, 1-11 min held
551 at 50% B and 0.1 mL/min, 11-11.05 min from 50% B to 0% B at 0.1 mL/min, 11.05-14 min held
552 at 0% B at 0.1 mL/min, 14-14.05 min held at 0% B and increased flow rate from 0.1 mL/min
553 to 0.25 mL/min, and 14.05-16 min held at 0% B and 0.25 mL/min. The mass spectrometer
554 acquisition settings were as follows: source voltage -2,500V, sheath gas 60, aux gas 19,
555 sweep gas 1, ion transfer tube temperature 320ºC, and vaporizer temperature 250ºC. Full
556 scan data were collected with a scan range of 70-800 m/z at a mass resolution of 240,000.
557 Fragmentation data was collected using a data-dependent MS2 (ddMS2) acquisition method
558 with MS1 mass resolution at 120,000, MS2 mass resolution at 15,000, and HCD collision
559 energy fixed at 30%.
560 Natural isotope abundance correction was done using the FluxFix Isotopologue Analysis
561 Tool*14* (version 0.1) web-based application[29]. Data analysis was conducted in Skyline (version
562 23.1.0.268), consisting of peak picking and integration, using an in-house curated compound
563 database of accurate mass MS1 and retention time derived from analytical standards and/or
564 MS2 spectral matches for the specified chromatography method.
565
566 ***AASDHPPT co-essentiality analysis and network modeling***
567 Gene essentiality scores and gene co-dependency Pearson correlation values were
568 obtained from the DepMap Portal Project Achilles 23Q4 release[14,30–32] in which genome-wide
569 CRISPR loss-of-function screens were performed in 1100 human cancer cell lines. Co-
570 Dependency plots between AASDHPPT and other genes were generated from gene
571 essentiality scores for each cancer line obtained directly from the DepMap Portal. For two-
572 dimensional network analysis, gene essentiality correlations for a custom list of genes were
573 used to create a data matrix (see Supplementary Excel File**)**. From this matrix, methodologies
574 and code originally published by Arnold et al.[33] and available at: https://github.com/finley-
575 lab/coessentiality-network were first used to generate a correlation matrix heatmap of
576 codependent gene modules. Co-dependent gene modules were then visualized as a network
577 diagram and genes with low correlation scores (Pearson r < 0.2) filtered out as previously

578 described[33]. Graph edges were weighted according to the strength of pairwise gene
579 correlations.
580
581 ***Relative quantification of NDUFAB1 species***
582 Method was adapted from the literature for use in our model[16,17]. Standards for NDUFAB1
583 modifications were synthesized as in reference 14 and digested with AspN (Sigma,
584 11420488001) overnight at 37°C in a ratio of 1:20 (w/w) enzyme to sample, buffered to a pH
585 of 7.6 with MOPS to a final concentration of 50mM. AspN digestion was quenched by the
586 addition of methanol to 50%. Digested standards were then pooled for detection by liquid-
587 chromatography mass spectrometry. For biological samples of NDUFAB1 species, ten 15-cm
588 dishes of approximately 40% confluent C2C12 cells from each genotype were transiently
589 transfected with either NDUFAB1-Flag or an empty vector control. After 48-hours cells were
590 washed with ice cold PBS and frozen at -80°C. After 16 hours at -80, cells were lysed with a
591 triton lysis buffer (1% triton, 10mM HEPES, 0.3mM EDTA, 120mM NaCl, and mammalian
592 protease inhibitor) on ice for 30 minutes. The samples were then spun at 17,000 x g at 4°C
593 for 30 minutes and cleared supernatants were incubated with anti-FLAG magnetic beads
594 (Sigma, M8823) for three hours at 4°C. After three hours, bound proteins were eluted from
595 beads using Flag peptide (Sigma, F4799) in elution buffer (10mM HEPES, 50mM NaCl,
596 mammalian protease inhibitor) for one hour at room temperature, filtered, and quantified via
597 Bradford assay (BioRad, 5000205). Protein that remained bound to beads was eluted with 1x
598 Laemmli buffer and run on an SDS-PAGE gel that then underwent Coomassie staining. As
599 determined by Bradford assay, three micrograms of Flag peptide-eluted protein from each
600 sample were digested with AspN as above. After digest was quenched with methanol,
601 samples were dried then resuspended in 50% methanol:50% water for further analysis by
602 mass spectrometry. Samples were analyzed with a Vanquish (Thermo Scientific) liquid
603 chromatography system coupled to an Orbitrap ID-X Tribrid mass spectrometer (Thermo
604 Scientific) in full scan mode for standards and with targeted simulated ion monitoring (tSIM)
605 for immunoprecipitation samples. For the chromatography approach, a reversed-phase C18
606 column (Agilent ZORBAX RRHS Extend-C18 Column, 759700-902) was used to separate
607 samples using acidic (0.1% formic acid) solvents, and the first 1.5 minutes of column eluants
608 were diverted to waste due to the presence of MOPS buffer in this time frame.
609 Chromatographic traces and peak areas were quantified from extracted ion chromatograms
610 of expected masses, matched to retention times from relevant standards using the software
611 FreeStyle (Thermo).

612

613 ***Cell immunostaining and microscopy analysis***

614 Cells were seeded into chambered cover glass slides and cultured overnight. The
615 following day, cells were fixed in ice-cold 4% paraformaldehyde (PFA) in PBS solution for 10
616 minutes at room temperature, followed by 3 washes in 1X PBS solution. Cells were then
617 permeabilized and blocked in PBS solution containing 0.5% BSA, 5% goat serum, and 0.3%
618 Triton X-100 for 1 hour at room temperature. Cells permeabilized/blocked with blocking buffer
619 were then incubated with denoted primary antibodies for one hour at room temperature
620 followed by washes with 1X PBS prior to incubation with Alexa Fluor conjugated secondary
621 antibodies (**Table 5**) for 2 hours at room temperature. Washes were repeated and cells were
622 then stained with Hoechst Dye for 10 minutes at room temperature. After subsequent washes,
623 samples were then imaged on a Zeiss LSM 880 with Airyscan and non-linear optics
624 microscope, using a 40X water objective and 1.2 NA to collect z-stacks, or with a Nikon Eclipse
625 T*i*2 epifluorescent microscope (20X objective, 0.75 NA or 60X oil immersion objective, 1.40
626 NA).

627 For quantification of endogenous AASDHPPT expression in control and *Aasdhppt* mutant
628 clonal lines, regions of interest (ROIs) were manually drawn with Fiji software for individual
629 cells from channels with fluorescent ATP5a expression. Area was then measured for each
630 ROI with corresponding mean fluorescent intensity of signal from the AASDHPPT fluorescent
631 channel. Mean fluorescent intensity per cell area was then calculated. For statistical analysis,
632 GraphPad Prism v10 software was used to remove outliers from the data set by the ROUT
633 method, Q = 1%.

634 For colocalization analysis of endogenous AASDHPPT or AASDHPPT-GFP fusion
635 constructs with mitochondrial proteins in maximum intensity projections of each imaged field,
636 nuclear signal detected by Hoechst Dye staining was first used to create ROIs in Fiji. Pixels
637 with signal detected in nuclear ROIs in red and green channels were then removed from
638 images of the same field prior to merging of red and green channels so that colocalization
639 analysis would be exclusive of nuclei and limited to subcellular organelles and cytoplasmic
640 regions. Merged channels were then processed by the BIOP JACoP Fiji plugin
641 (https://c4science.ch/w/bioimaging_and_optics_platform_biop/image-
642 processing/imagej_tools/jacop_b/) using the Otsu method of thresholding for each channel to
643 generate Pearsons Correlation values.

644

645 ***Bimolecular fluorescence complementation (BiFC) assay***

646 To generate BiFC cell lines, five split-Venus constructs were designed and synthesized by
647 VectorBuilder in a pMMLV retroviral backbone. Constructs were designed to contain either the
648 C' terminal half of the Venus tag with blasticidin resistance (VC), or the N' terminal half of the
649 Venus tag with puromycin resistance (VN). VC constructs were tagged to the C' terminal end
650 of *citrate synthase* (CS-VC), *mitofusin 2* (MFN2-VC) or *Ndufab1* (NDUFAB1-VC). VN
651 constructs were tagged to either the C' or N' terminal end of *Aasdhppt* (PPT-VN and VN-PPT,
652 respectively). Following retroviral packaging in HEK293T cells, 40,000 wildtype C2C12 cells
653 were transduced to express either PPT-VN or VN-PPT in combination with each VC construct.
654 Negative control lines were generated by transducing cells with individual VC or VN constructs
655 alongside an empty vector control (PQXCIP for VC constructs, and PQXCIB for VN
656 constructs). This ensured that all cells were transduced with an approximately equal total viral
657 load. Stable populations were derived via combined puromycin and blasticidin selection (2
658 µg/mL each), yielding 11 cell lines in total; 6 with combined VC/VN constructs plus 5 single
659 construct controls.
660 For measurement of fluorescence, approximately 100,000 cells were trypsinized and
661 resuspended in 200 µL PBS. Cell suspensions were then assessment on an Accuri bench-top
662 cytometer, recording a minimum of 20,000 events per sample. The percentage of Venus-
663 positive cells was analyzed using FlowJo (v. 10.10.0). Fluorescence intensity histograms were
664 generated using FlowJo Layout Editor. A representative flow cytometry gating strategy is
665 shown in Extended data Fig. 3C. Visual confirmation of fluorescence achieved by imaging all
666 BiFC cell lines on a Nikon Eclipse Ti2 microscope. Briefly, 20,000 cells per cell line were
667 seeded in chamber cover slides (Cellvis, C4-1.5H-N). After 24 hours, cells were fixed in 4%
668 PFA for 30 mins at room temperature before imaging the following day (20X objective, 0.75
669 NA).
670
671 ***Statistics***
672 Statistical analysis was performed using GraphPad Prism 10. Unless otherwise noted,
673 data were analyzed by one-way ANOVA followed by two-sided Dunnett's multiple comparison
674 test (when compared to only control) or Šídák's or Tukey's multiple comparison test (when
675 comparing all groups). A p-value of <0.05 was considered statistically significant. Data that
676 included a third variable (ex. time) was analyzed by two-way ANOVA followed by Tukey's
677 multiple comparison test.
678
679 **Table 1**

sgRNA cloned into pLentiCRISPRv2	sequence
PPT 1	GATGCGGTCTATCCAGCCGG
PPT 2	GCAGACGGATATGATCCCAA
PPT 3	AGCGGACCGAGCCGGTCGTA
PPT 4	GGAACACCATACGACCGGCT

680

681

682 **Table 2**

siRNA target	ID#	Sequence
Aasdhppt #1	Thermo Fisher Scientific s85366	CGUUGAAUCCAUAUCCCAAtt
Aasdhppt #2	Thermo Fisher Scientific s85364	GGACUCAGCUGGAUAUGUUtt
Ndufab1 Pooled	Horizon Discovery L-055864-01-0005	CACUGACGUUAGACGGAAU
		CAGAAAAGCUCUCCGUAAA
		CUGAAGAAUUGGCGCAAAA
		GGAUGUGUAUGAAUAAAGU

683

684

685 **Table 3**

Primers for site-directed mutagenesis	sequence
P12S Fwd	GTGCGTGGTGAGCTCCATGGAGG
P12S Rev	AGCCTCTTAGCGGGG
R47H Fwd	GGAGAAGGAGCATATCGGCAAGTTC
R47H Rev	TCCGGCTGGATAGAC
A72T Fwd	GAAATTAGTTACCGAGAAATTGAATATCCC
A72T Rev	CTTATCATCAAACGACCAG
W79G Fwd	GAATATCCCTGGCGATCATATCCGTC
W79G Rev	AATTTCTCTGCAACTAATTTC
R83C Fwd	GGATCATATCTGCCTGCAGAGAAC
R83C Rev	CAAGGGATATTCAATTTCTC

K96E Fwd	GGTTCTTGCGGAAGACTCGTTGA
K96E Rev	GGCTTTCCCTTTGAAGTTCTC
NDUFAB1 S112A Fwd	GGGCTTAGACGCTTTGGACCAAGTG
NDUFAB1 S112A Rev	AGGTCTTTCATAAAATGAGAATTTAC

686

687 **Table 4**

688

Primers for Genomic Amplification of *Aasdhppt*	
Forward Primer	TACCTGGCTTGAGGATCAGC
Reverse Primer	GGTTCTGCAGCAAGAACTGCAT

689

690

691 **Table 5**

Antibodies	**Source and reference number**
AASDHPPT	Proteintech 11244-1-AP
β-actin	Proteintech 66009-1-Ig
NDUFA9	Abcam ab14713
UQCRFS1	Proteintech 18443-1-AP
MTCO1	Abcam ab110270
ATP5a	Abcam ab14748
Lipoic acid	Millipore 437695
Pyruvate Dehydrogenase E2 (DLAT)	Abcam ab172617
DLST	Cell Signaling 5556
SDHB	Abcam ab14714
NDUFAB1	Abcam ab96230 and ab181021
GFP	Abcam ab290
Citrate Synthase	Cell Signaling 14309
Anti-V5	Abcam ab27671
Anti-FLAG	Thermo Fisher MA1-91878
MECR	Proteintech 51027-2-AP
Goat anti-Mouse IgG (H+L) AlexaFluor 568	Thermo Fisher A-11004
Goat anti-Mouse IgG (H+L) Alexafluor 488	Thermo Fisher A-11029
Goat anti-Rabbit IgG (H+L) AlexaFluor 568	Thermo Fisher A-11011

Goat anti-Mouse IgG (H+L), HRP	Thermo Fisher A28177
Goat anti-Rabbit IgG (H+L), HRP	Thermo Fisher A16110
Goat anti-Mouse IgG (H+L) Dylight 800	Rockland Immunochemicals 610-145-002-0.5
Goat anti-Rabbit IgG (H+L) Dylight 800	Rockland Immunochemicals 611-145-002-0.5
Goat anti-Mouse IgG (H+L) AlexaFluor 680	Thermo Fisher A-21057
Goat anti-Rabbit IgG (H+L) AlexaFluor 680	Thermo Fisher A10043

Acknowledgments

This work was supported by funding from the NIH (R35GM151245 to SMN) and the Van Andel Institute – Metabolism & Nutrition (MeNu) Program. Stipend support for RJW and OAP was provided by the Van Andel Institute Graduate School (VAIGS). RJW was also supported by NIH F30GM154476. We thank the Meijer Foundation for financial support of MC and EM. We also thank the Van Andel Institute's Flow Cytometry Core (RRID:SCR_022685) for their assistance with single cell sorting for generation of clonal cell lines, the Metabolomics and Mass Spectrometry Core (RRID:SCR_024903) for their assistance with labeled glutamine tracing experiments and analysis as well as method development for the direct relative quantification of NDUFAB1 acylation species, the Optical Imaging Core (RRID:SCR_021968) for their assistance with airyscan microscopy, and the Bioinformatics and Biostatistics Core (RRID:SCR_024762) for their assistance with gene essentiality score correlation network analysis.

Author Contributions

Conceptualization: PRN, RJW, SMN; Methodology: PRN, RJW, MC; Investigation: PRN, RJW, SEJP, MC, NG, JZL, OAP, EM; Formal Analysis: PRN, RJW, SEJP; Funding acquisition: RJW, SMN; Resources: SMN; Supervision: SMN; Visualization: PRN, RJW, SEJP; Writing – original draft: PRN, RJW, JZL, SMN; Writing – review & editing: PRN, RJW, SEJP, MC, OAP, MLH, SMN

The authors declare no competing interests.

Data Availability

All data needed to evaluate the conclusions in the manuscript are present in the manuscript and/or Supplementary Information. Additional data related to this paper may be requested from the authors.

Figure Legends

Figure 1. AASDHPPT is required for mitochondrial oxidative metabolism.
(A) Whole cell lysates were separated by SDS-PAGE and immunoblotted for the denoted targets in clonal control, *Aasdhppt*-deficient, and siRNA-transfected cells. Data are representative of 3 biological replicates. (B-C) Cells were grown in either 25 mM glucose (B) or 10 mM galactose (C) in an IncuCyte® system with images captured every 3 hours for 4 days or 2 days respectively. Data represent the mean doubling time calculated from technical replicates of growth curves; error bars denote SEM **** = $p < 0.0001$. Data are representative of 1 experiment from $n > 3$ biological replicates. (D) Seahorse mitochondrial stress test for Oxygen Consumption Rate (OCR) of indicated cell lines expressing mtDSRed or PPT-GFP. Data are representative of 1 experiment from 3 biological replicates. Error bars represent SD. Significance determined at indicated time points using one-way ANOVA, **** = $p < 0.0001$ (E) Blue-native PAGE separation of isolated mitochondrial protein complexes from denoted cell lines expressing mtDSRed or PPT-GFP, followed by immunoblot with the indicated antibodies. Data are representative of $n > 3$ biological replicates. (F) Schematic of isotopomeric labeling patterns upon substitution of $U^{13}C$-glutamine for unlabeled glutamine. Open circles indicate ^{12}C carbons, where circles with grey, red, or blue, indicate ^{13}C carbons. (G-H) Technical triplicate samples (n=3) of the indicated cell lines cultured in $U^{13}C$-glutamine for the indicated time points, harvested, and analyzed via LC-MS. Steady state metabolite pool sizes and ratios are shown for the 4-hour labeling time point. (I) Ratio of Citrate M+5 to Citrate M+4 at the four-hour time point. Error bars represent SEM (B, C), SD (D, G, H, I). ** = $p<0.01$, *** = $p<0.001$, **** = $p<0.0001$ as determined by ANOVA followed by Tukey's multiple comparisons test.

Figure 2. AASDHPPT is required for mitochondrial fatty acid synthesis pathway function.
(A) Two-dimensional network diagram representing gene essentiality score correlations between selected genes associated with *AASDHPPT* and known substrate targets, mtFAS pathway members, LYRM family members, and the GO term "pantothenate metabolism" using

752 a minimum threshold correlation score > 0.2. Different colors represent genes associated with
753 clusters as shown in Extended Data Fig. 2E. Correlation strength is represented by the length
754 and thickness of the connecting edge. (B) Whole cell lysates from indicated cell lines
755 expressing mtDSRed or PPT-GFP fusion protein were separated by SDS-PAGE and
756 immunoblotted for the denoted targets. Data are representative of 3 biological replicates. Red
757 asterisk denotes ATP5a band from previous blot. (C) Whole cell lysates from indicated cell
758 lines expressing either NDUFAB1-Flag or NDUFAB1$_{S112A}$-Flag were separated by SDS-PAGE
759 and immunoblotted for protein expression of the denoted targets. Data are representative of
760 3 biological replicates. (D) Schematic of mass spectrometry approach using AspN digestion
761 to detect Apo-, Holo-, and Acyl- species of NDUFAB1. (E) Coomassie stain of SDS-PAGE gel
762 of NDUFAB1-FLAG immunoprecipitation from the indicated cell line. (F) Relative
763 quantification of NDUFAB1 AspN digest products via tandem liquid chromatography mass
764 spectrometry n=3 technical replicates from immunoprecipitation, representative of 3 distinct
765 biological replicates. NS = not significant, *** = p<0.001, **** = p<0.0001 as determined by
766 two-way ANOVA followed by Šidák's multiple comparisons test. (G) Representative overlayed
767 extracted ion chromatograms of Apo-, Holo-, and Acyl-NDUFAB1 from cells of the indicated
768 genotype, quantified in F.
769
770 **Figure 3. AASDHPPT localizes to the mitochondrial matrix.**
771 (A) Representative 40X HPF images of the indicated cell lines immunostained with
772 Hoechst dye to visualize nuclei and antibodies against AASDHPPT (red) and ATP5a (green).
773 Scale bars = 100μm. (B) Quantification of AASDHPPT and ATP5a signal colocalization
774 outside of the nucleus from n = 8 40X HPF per group assessed by Pearson's correlation
775 coefficient. (C) Subcellular fractionation of *Aasdhppt* mutant cell lines and control. Post-
776 mitochondrial supernatant (PMS) and mitochondrial lysate (Mito) was isolated from the
777 indicated cell lines and immunoblotted for denoted targets. Data are representative of 3
778 biological replicates. (D) Representative 40X HPF images of WT skeletal muscle myoblasts
779 expressing AASDHPPT-GFP (PPT-GFP) stained with Hoechst dye and antibody against
780 ATP5a (red). Scale bars represent 100 μm. Dashed outlines denote magnified regions shown
781 in panels with solid outlines. For all statistical analysis data represent the mean; error bars
782 denote SD. **** = p<0.0001 as determined by one-way ANOVA with Šidák's multiple
783 comparisons test. (E) Representative histograms of Venus (FITC) fluorescence in the
784 indicated BiFC cell lines. (F) Percentage of Venus-positive cells in the indicated cell lines as
785 measured by flow cytometry. Data represent the mean; error bars denote standard deviation

786 (n = 3 per group). Statistical significance was determined by one-way ANOVA with Tukey's
787 multiple comparison test. (G) Representative 20X images of endogenous Venus fluorescence
788 in VC + VN BiFC cell lines. Scale bars represent 50 μm.
789
790 **Figure 4. AASDHPPT has a N-terminal MTS**
791 (A) Schematic Illustration of MitoFates[20] predicted features in full length AASDHPPT
792 (PPT-GFP) and AASDHPPT with a 1-13 (Δ1-13) or 1-36 (Δ1-36) N-terminal truncation. (B)
793 Quantification of MTS presequence probability in AASDHPPT, NDUFAB1, Citrate Synthase
794 (CS) and Mitofusin 2 (MFN2) determined by MitoFates. (C) Representative 40X HPF images
795 of WT cells expressing mtDSRed, PPT-GFP, 13 residue N-terminal truncation of PPT ($PPT_{\Delta 1-}$
796 $_{13}$-GFP), or 36 residue N-terminal truncation of PPT ($PPT_{\Delta 1-36}$-GFP) constructs, stained with
797 Hoechst dye and antibody against ATP5a (red). Scale bars represent 100 μm. Arrows denote
798 weak expression of GFP signal detected. (D) Quantification of PPT-GFP and ATP5a signal
799 colocalization outside of the nucleus from n = 8 40X HPF assessed by Pearson's correlation
800 coefficient from experiment shown in (C). Data represent the mean; error bars denote SD. ****
801 = p<0.0001, determined by one-way ANOVA with Dunnett's multiple comparisons test. (E)
802 Subcellular fractionation of WT cells expressing PPT-GFP, $PPT_{\Delta 1-13}$-GFP, or $PPT_{\Delta 1-36}$-GFP.
803 Post-mitochondrial supernatant (PMS) and mitochondrial lysate (Mito) was isolated from the
804 denoted cell lines, separated by SDS-PAGE, and immunoblotted for the indicated targets.
805 Data are representative of 3 biological replicates. (F) Representative histograms of Venus
806 (FITC) fluorescence in the indicated BiFC cell lines. (G) Percentage of Venus-positive cells in
807 the indicated cell lines as measured by flow cytometry. Data represent the mean; error bars
808 denote standard deviation (n = 3 per group). Statistical significance was determined by one-
809 way ANOVA with Tukey's multiple comparison test. **** = p<0.0001
810
811 **Figure 5. Mitochondrial localization of AASDHPPT is required for mtFAS function.**
812 (A) Whole cell lysates from cells expressing mtDSRed, PPT-GFP, $PPT_{\Delta 1-13}$-GFP, or $PPT_{\Delta 1-}$
813 $_{36}$-GFP were separated by SDS-PAGE and immunoblotted for the denoted targets. Data are
814 representative of n > 3 biological replicates. (B) Blue-native PAGE separation of isolated
815 mitochondrial protein complexes from denoted cell lines expressing mtDSRed, PPT-GFP, or
816 $PPT_{\Delta 1-13}$-GFP, followed by immunoblot with the indicated antibodies. Data are representative
817 of n > 3 biological replicates. (C) Seahorse mitochondrial stress test for Oxygen Consumption
818 Rate (OCR) of indicated cell lines expressing mtDSRed, PPT-GFP, or $PPT_{\Delta 1-13}$-GFP. Data are

819 representative of 1 experiment from 3 biological replicates. Error bars represent SD. (D)
820 Quantification of basal respiration, ATP-production coupled respiration, maximal respiration
821 and proton leak from data in (C). Data are mean OCR; error bars are SEM. **** = p <0.0001,
822 determined by one-way ANOVA with Tukey's multiple comparisons test. (E) Whole cell lysates
823 from clonal control, *Aasdhppt*-, and *Mecr*-deficient cells expressing mtDSRed or yPpt2-V5
824 were separated by SDS-PAGE and immunoblotted for the denoted targets. Data are
825 representative of 3 biological replicates. (F) Whole cell lysates from the indicated cell lines
826 expressing mtDSRed, PPT-GFP P12S, PPT-GFP R47H, PPT-GFP A72T, PPT-GFP W79G,
827 PPT-GFP R83C, or PPT-GFP K96E were separated by SDS-PAGE and immunoblotted for
828 the denoted targets. Immunoblots are representative of 3 biological replicates. (G) Seahorse
829 mitochondrial stress test for Oxygen Consumption Rate (OCR) of indicated cell lines
830 expressing mtDSRed, PPT-GFP, PPT-GFP R47H, PPT-GFP A72T, PPT-GFP W79G, PPT-
831 GFP R83C, or PPT-GFP K96E. Data are representative of 1 experiment from 3 biological
832 replicates. Error bars represent SD. (H) Quantification of basal respiration, ATP-production
833 coupled respiration, maximal respiration and proton leak from data in (G). Data are mean
834 OCR; error bars are SEM. ** = p <0.01, *** = p < 0.001, **** = p <0.0001, determined by one-
835 way ANOVA with Šidák's multiple comparisons test.
836
837 **Extended Data Fig. 1. AASDHPPT is required for mitochondrial oxidative metabolism.**
838 ((A) Sequence analysis sgRNA-targeted regions PCR-amplified and subcloned into
839 pCR™4-TOPO plasmid in clonal *Aasdhppt* mutant cell lines, and corresponding mutations
840 sequenced. (B-C) Cells were grown in either 25 mM glucose (B) or 10 mM galactose (C) in
841 an IncuCyte® system with images captured every 3 hours for 4 or 2 days respectively. Data
842 represent the mean doubling time calculated from technical replicates of growth curves; error
843 bars denote SEM, **** = p <0.0001 as determined by one-way ANOVA with Tukey's multiple
844 comparisons test. Data are representative of 1 experiment from n > 3 biological replicates.
845 (D) Seahorse mitochondrial stress test for Oxygen Consumption Rate (OCR) of indicated cell
846 lines. Data are representative of 1 experiment from 3 biological replicates. Error bars
847 represent SD. Significance determined at indicated time points using one-way ANOVA, **** =
848 p <0.0001 (E) Blue-native PAGE separation of isolated mitochondrial protein complexes from
849 denoted cell lines, followed by immunoblot with the indicated antibodies. Data are
850 representative of n > 3 biological replicates. (F-J) Pool size of the indicated metabolites from
851 steady state metabolomics analysis at the four-hour labeling time point. Data from n=3
852 technical replicates of the indicated cell lines. Error bars represent SD. Statistical analysis was

853 done using a one-way ANOVA followed by Tukey's multiple comparisons test. (K-L) Fractional
854 enrichment of given isotopologues is represented as percentage of the total pool at each
855 indicated time point. Error bars represent SD. Significance was determined by two-way
856 ANOVA followed by Tukey's multiple comparisons test. ** = p <0.01. *** = p <0.001. **** = p
857 <0.0001. NS = not significant.
858
859 **Extended Data Fig. 2. AASDHPPT is required for mitochondrial fatty acid synthesis**
860 **pathway function.**
861 (A-D) Codependency plots of gene essentiality scores comparing *AASDHPPT* with
862 *NDUFAB1* (A), *OXSM* (B), *MCAT* (C), and *MECR* (D) from DepMap CRISPR screens[14,30–32,34]**.**
863 **(**E) Heatmap depicting hierarchical clustering of pairwise gene essentiality score correlations
864 of PPT, known PPT substrate targets, mtFAS pathway members, LYRM family members, and
865 genes associated with the GO term "pantothenate metabolism." (F) CoA pool size in cells of
866 the indicated genotype. Statistical analysis performed via one-way ANOVA with Tukey's
867 multiple comparisons. ** = p <0.01, other p values as written. (G) Whole cell lysates from WT
868 cells transfected with siRNAs targeting *Aasdhppt, Ndufab1*, or scramble control were
869 separated by SDS-PAGE and immunoblotted for the denoted targets. Data are representative
870 of 3 biological replicates. H) Representative extracted ion chromatograms for indicated
871 NDUFAB1 species from control cell line overlayed with extracted ion chromatograms from a
872 pool of Apo- Holo- and Acyl- standards run with identical chromatography. Standards were run
873 in full scan mode while samples were run with targeted selective ion monitoring.
874
875 **Extended Data Fig. 3. AASDHPPT localizes to the mitochondrial matrix**
876 (A) Representative 40X HPF images of the indicated cell lines stained with Hoechst dye
877 and antibodies against AASDHPPT (red) and ATP5a (green). Scale bars = 100μm. (B)
878 Quantification of mean fluorescent intensity of AASDHPPT expression per cell area (μm^2) in
879 *Aasdhppt* mutants (PPT-1 n = 170 and PPT-2 n =159) and control clonal cell lines (Ctrl-1 n =
880 186 and Ctrl-2 n = 118) as represented in A and Fig. 3A. (C) Representative 60X HPF images
881 of WT cells stained with Hoechst dye and antibodies against AASDHPPT (red) and ATP5a
882 (green) along with secondary antibody-only controls. Scale bars are 25 μm. (D)
883 Representative 20X HPF images of WT cells transfected with the denoted siRNAs following
884 fixation at 72 hours post-transfection. Cells were stained with Hoechst dye and antibodies
885 against AASDHPPT (red) and ATP5a (green). Scale bars are 50 μm. (E) Representative 60X
886 HPF images of WT cells expressing AASDHPPT-Flag (PPT-Flag) stained with Hoechst dye

887 and antibodies against Citrate Synthase (red) and Flag-tag (green) along with secondary
888 antibody-only controls (AF-568 and AF-488). Scale bars are 25 μm. (F) Representative
889 schematic of flow cytometry gating strategy for experiments in Fig. 3E-F.
890
891 **Extended Data Fig. 4. AASDHPPT has a N-terminal MTS**
892 (A) Sequence alignment: MTS conservation. Accession numbers as follows; *Mus*
893 *musculus:* NP_001313288.1, *Homo sapiens: NP_056238.2, Rattus norvegicus:*
894 *NP_001100268.2, Danio rerio: NP_001028901.1, Gallus gallus: NP_001265017.1*. (B)
895 Representative 60X HPF images of WT cells expressing PPT-GFP, 13 residue N-terminal
896 truncation of PPT ($PPT_{\Delta 1\text{-}13}$-GFP), or 20 residue N-terminal truncation of PPT ($PPT_{\Delta 1\text{-}20}$-GFP)
897 constructs, stained with Hoechst dye and antibody against ATP5a (red). Scale bars are 25
898 μm. (C) Representative 60X HPF images of cells expressing PPT MTS-GFP stained with
899 Hoechst dye and antibody against ATP5a (red). Scale bars represent 20 μm. (D) Subcellular
900 fractionation of cells expressing PPT MTS-GFP. Post-mitochondrial supernatant (PMS) and
901 mitochondrial lysate (Mito) was isolated, separated by SDS-PAGE, and immunoblotted for the
902 indicated targets. Blots are representative of 3 biological replicates.
903
904 **Extended Data Fig. 5. Mitochondrial localization of AASDHPPT is required for mtFAS**
905 **function**
906 (A) Whole cell lysates from cells expressing mtDSRed, PPT-GFP, $PPT_{\Delta 1\text{-}13}$-GFP, or $PPT_{\Delta 1\text{-}}$
907 $_{36}$-GFP were separated by SDS-PAGE and immunoblotted for the denoted targets. Data are
908 representative of n > 3 biological replicates. (B) Blue-native PAGE separation of isolated
909 mitochondrial protein complexes from denoted cell lines expressing mtDSRed, PPT-GFP, or
910 $PPT_{\Delta 1\text{-}13}$-GFP, followed by immunoblot with the indicated antibodies. Data are representative
911 of n > 3 biological replicates. (C) Seahorse mitochondrial stress test for Oxygen Consumption
912 Rate (OCR) of indicated cell lines expressing mtDSRed, PPT-GFP, or $PPT_{\Delta 1\text{-}13}$-GFP. Data are
913 representative of 1 experiment from 3 biological replicates. Error bars represent SD. (D)
914 Quantification of basal respiration, ATP-production coupled respiration, maximal respiration
915 and proton leak from data in (C). Data are mean OCR; error bars are SEM. * = $p < 0.05$, ** =
916 $p < 0.01$, *** = $p < 0.001$, **** = $p < 0.0001$, determined by one-way ANOVA with Tukey's
917 multiple comparisons test. (E) Subcellular fractionation of clonal control cells expressing
918 yPpt2-V5. Post-mitochondrial supernatant (PMS) and mitochondrial lysate (Mito) was
919 isolated, separated by SDS-PAGE, and immunoblotted for the indicated targets. Data are
920 representative of 3 biological replicates. (F) Whole cell lysates from clonal control *and* Mecr-

921 deficient cells were separated by SDS-PAGE and immunoblotted for the denoted targets. Data
922 are representative of 3 biological replicates. (G) Whole cell lysates from indicated cell lines
923 expressing mtDSRed, PPT-GFP P12S, PPT-GFP R47H, PPT-GFP A72T, PPT-GFP W79G,
924 PPT-GFP R83C, or PPT-GFP K96E were separated by SDS-PAGE and immunoblotted for
925 the denoted targets. Immunoblots are representative of n>3 biological replicates. (H)
926 Representative 60X HPF images of WT cells expressing PPT-GFP, PPT-GFP R47H, PPT-
927 GFP A72T, PPT-GFP W79G, PPT-GFP R83C, or PPT-GFP K96E stained with Hoechst Dye
928 and antibody against ATP5a (red). Scale bars represent 25 μm.
929
930 **References**

931 1. Chen, N., Liu, Y., Li, Y. & Wang, C. Chemical Proteomic Profiling of Protein 4'-
932 Phosphopantetheinylation in Mammalian Cells. *Angew. Chem. Int. Ed Engl.* **59**, 16069–
933 16075 (2020).
934 2. Joshi, A. K., Zhang, L., Rangan, V. S. & Smith, S. Cloning, Expression, and
935 Characterization of a Human 4′-Phosphopantetheinyl Transferase with Broad Substrate
936 Specificity*. *J. Biol. Chem.* **278**, 33142–33149 (2003).
937 3. Stuible, H. P., Meier, S., Wagner, C., Hannappel, E. & Schweizer, E. A novel
938 phosphopantetheine:protein transferase activating yeast mitochondrial acyl carrier
939 protein. *J. Biol. Chem.* **273**, 22334–22339 (1998).
940 4. Guan, X. *et al.* A phosphopantetheinyl transferase that is essential for mitochondrial fatty
941 acid biosynthesis. *Plant J.* **84**, 718–732 (2015).
942 5. Fischer, U., Ludwig, N., Raslan, A., Meier, C. & Meese, E. Gene amplification during
943 myogenic differentiation. *Oncotarget* **7**, 6864–6877 (2016).
944 6. Zacharaki, P., Stephanou, G. & Demopoulos, N. A. Comparison of the aneugenic
945 properties of nocodazole, paclitaxel and griseofulvin in vitro. Centrosome defects and
946 alterations in protein expression profiles. *J. Appl. Toxicol.* **33**, 869–879 (2013).
947 7. Mullen, A. R. *et al.* Reductive carboxylation supports growth in tumour cells with defective
948 mitochondria. *Nature* **481**, 385–388 (2011).

949 8. Mullen, A. R. *et al.* Oxidation of alpha-ketoglutarate is required for reductive carboxylation
950 in cancer cells with mitochondrial defects. *Cell Rep.* **7**, 1679–1690 (2014).
951 9. Nowinski, S. M. *et al.* Mitochondrial fatty acid synthesis coordinates oxidative metabolism
952 in mammalian mitochondria. *Elife* **9**, e58041 (2020).
953 10. Tsherniak, A. *et al.* Defining a cancer dependency map. *Cell* **170**, 564-576.e16 (2017).
954 11. Wainberg, M. *et al.* A genome-wide atlas of co-essential modules assigns function to
955 uncharacterized genes. *Nat. Genet.* **53**, 638–649 (2021).
956 12. Solmonson, A. & DeBerardinis, R. J. Lipoic acid metabolism and mitochondrial redox
957 regulation. *J. Biol. Chem.* **293**, 7522–7530 (2018).
958 13. Van Vranken, J. G. *et al.* ACP Acylation Is an Acetyl-CoA-Dependent Modification
959 Required for Electron Transport Chain Assembly. *Mol. Cell* **71**, 567-580.e4 (2018).
960 14. DepMap, B. DepMap 23Q4 Public. Figshare+
961 https://doi.org/10.25452/FIGSHARE.PLUS.24667905.V2 (2023).
962 15. Wedan, R. J., Longenecker, J. Z. & Nowinski, S. M. Mitochondrial fatty acid synthesis is
963 an emergent central regulator of mammalian oxidative metabolism. *Cell Metab.* **36**, 36–
964 47 (2024).
965 16. Nam, J.-W. *et al.* A General Method for Quantification and Discovery of Acyl Groups
966 Attached to Acyl Carrier Proteins in Fatty Acid Metabolism Using LC-MS/MS. *Plant Cell*
967 **32**, 820–832 (2020).
968 17. Kim, D. *et al.* Mitochondrial NADPH fuels mitochondrial fatty acid synthesis and lipoylation
969 to power oxidative metabolism. *Nat. Cell Biol.* **27**, 790–800 (2025).
970 18. Kerppola, T. K. Design and implementation of bimolecular fluorescence complementation
971 (BiFC) assays for the visualization of protein interactions in living cells. *Nat. Protoc.* **1**,
972 1278–1286 (2006).
973 19. Omura, T. Mitochondria-targeting sequence, a multi-role sorting sequence recognized at
974 all steps of protein import into mitochondria. *J. Biochem.* **123**, 1010–1016 (1998).

975 20. Fukasawa, Y. *et al.* MitoFates: improved prediction of mitochondrial targeting sequences
976 and their cleavage sites. *Mol. Cell. Proteomics* **14**, 1113–1126 (2015).
977 21. Savojardo, C., Bruciaferri, N., Tartari, G., Martelli, P. L. & Casadio, R. DeepMito: accurate
978 prediction of protein sub-mitochondrial localization using convolutional neural networks.
979 *Bioinformatics* **36**, 56–64 (2020).
980 22. Savojardo, C., Martelli, P. L., Tartari, G. & Casadio, R. Large-scale prediction and analysis
981 of protein sub-mitochondrial localization with DeepMito. *BMC Bioinformatics* **21**, 266
982 (2020).
983 23. Webb, B. D. *et al.* Recessive pathogenic variants in MCAT cause combined oxidative
984 phosphorylation deficiency. *Elife* **12**, (2023).
985 24. Landrum, M. J. *et al.* ClinVar: improving access to variant interpretations and supporting
986 evidence. *Nucleic Acids Res.* **46**, D1062–D1067 (2018).
987 25. Naquet, P., Kerr, E. W., Vickers, S. D. & Leonardi, R. Regulation of coenzyme A levels by
988 degradation: the “Ins and Outs.” *Prog. Lipid Res.* **78**, 101028 (2020).
989 26. Kastaniotis, A. J., Autio, K. J. & R Nair, R. Mitochondrial fatty acids and neurodegenerative
990 disorders. *Neuroscientist* **27**, 143–158 (2021).
991 27. Lambrechts, R. A. *et al.* CoA-dependent activation of mitochondrial acyl carrier protein
992 links four neurodegenerative diseases. *EMBO Mol. Med.* **11**, e10488 (2019).
993 28. Sanjana, N. E., Shalem, O. & Zhang, F. Improved vectors and genome-wide libraries for
994 CRISPR screening. *Nat. Methods* **11**, 783–784 (2014).
995 29. Trefely, S., Ashwell, P. & Snyder, N. W. FluxFix: automatic isotopologue normalization for
996 metabolic tracer analysis. *BMC Bioinformatics* **17**, 485 (2016).
997 30. Meyers, R. M. *et al.* Computational correction of copy number effect improves specificity
998 of CRISPR–Cas9 essentiality screens in cancer cells. *Nat. Genet.* **49**, 1779–1784 (2017).
999 31. Dempster, J. M. *et al.* Extracting biological insights from the project Achilles genome-
1000 scale CRISPR screens in cancer cell lines. *bioRxiv* (2019) doi:10.1101/720243.

1001 32. Dempster, J. M. *et al.* Chronos: a CRISPR cell population dynamics model. *bioRxiv*
1002 (2021) doi:10.1101/2021.02.25.432728.
1003 33. Arnold, P. K. *et al.* A non-canonical tricarboxylic acid cycle underlies cellular identity.
1004 *Nature* **603**, 477–481 (2022).
1005 34. Pacini, C. *et al.* Integrated cross-study datasets of genetic dependencies in cancer. *Nat.*
1006 *Commun.* **12**, 1661 (2021).

FIGURE 1: AASDHPPT is a major determinant of mitochondrial oxidative metabolism

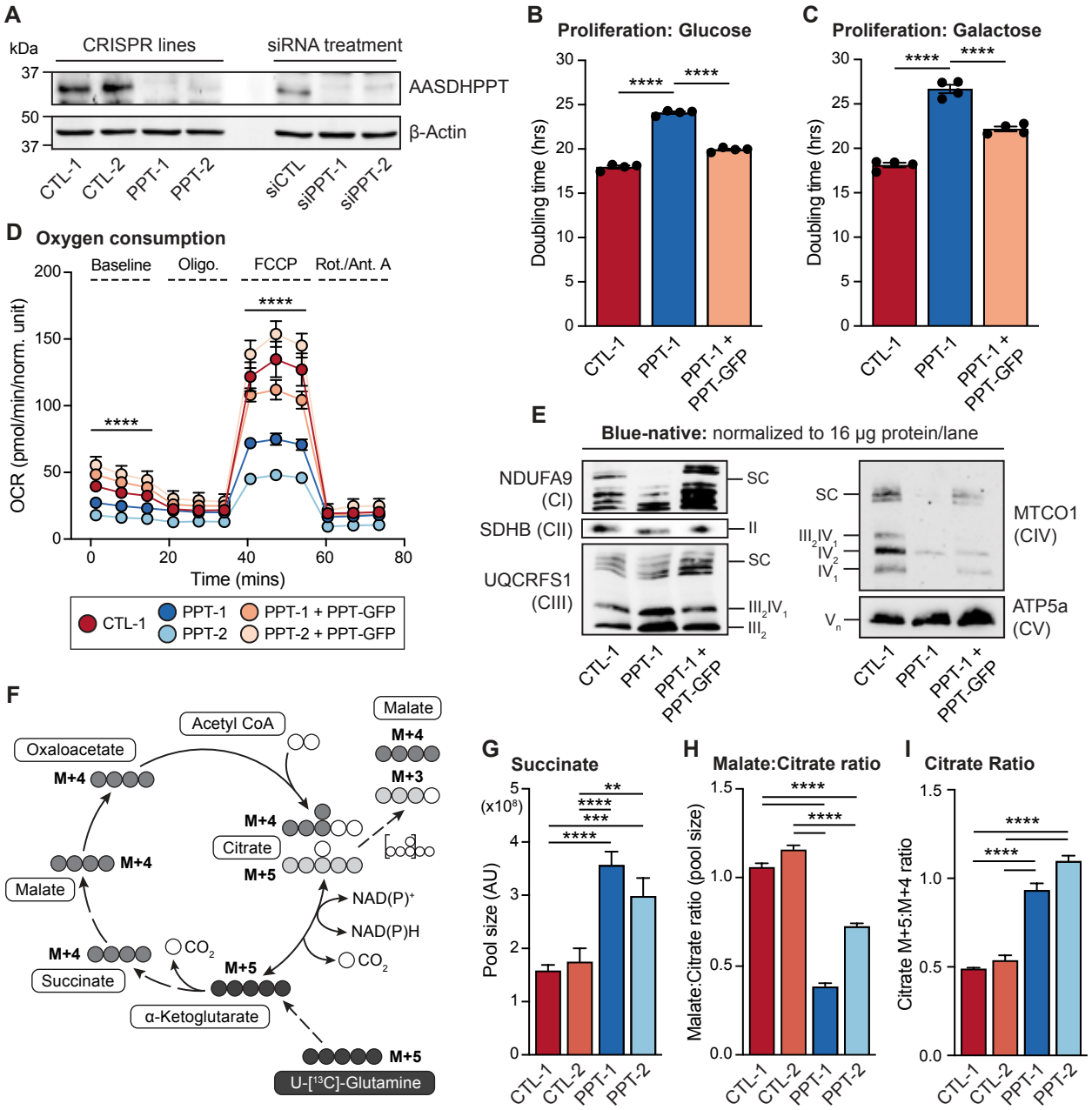

EXTENDED DATA FIGURE 1: AASDHPPT is a major determinant of mitochondrial oxidative metabolism

A PPT-1/2 mutations

Cell line	NC_000075.7	Protein
PPT-1	c.202_204delCAG	p.Q41del
	c.201_204delCCAG	p.Q41fs
	c.201_205delCCAGC	p.Q41fs
PPT-2	c.201_204delCCAG	p.Q41fs
	c.206_211delCGGAGG	p.P42Q p.E43del p.E44del
	No mutation	No mutation

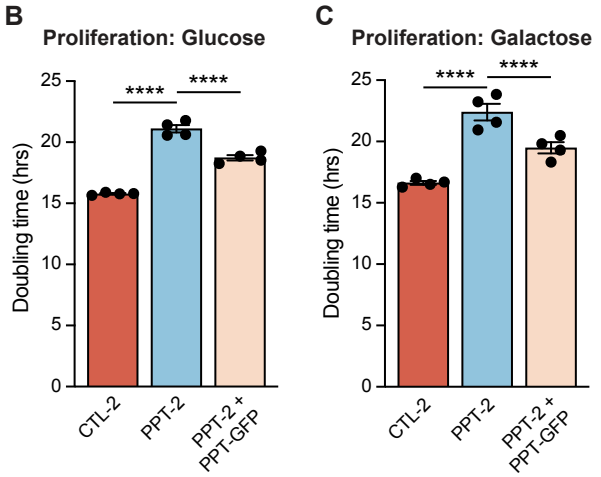

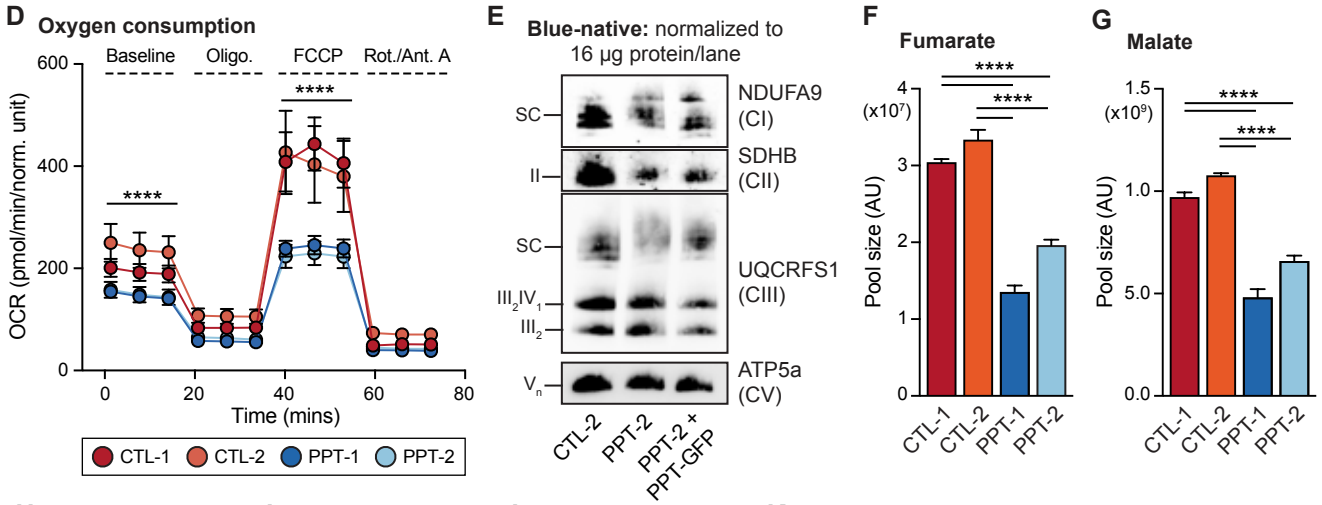

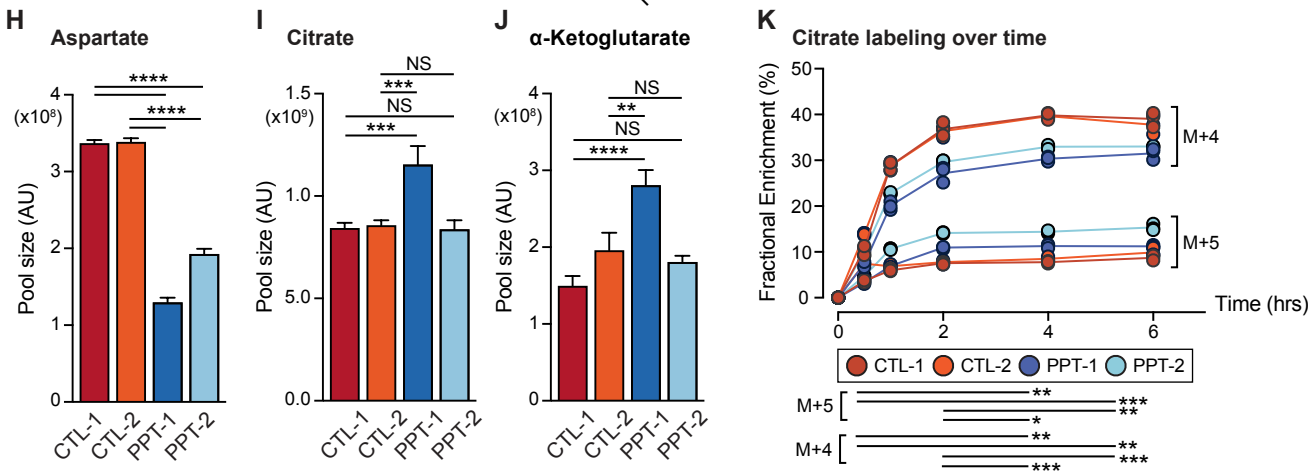

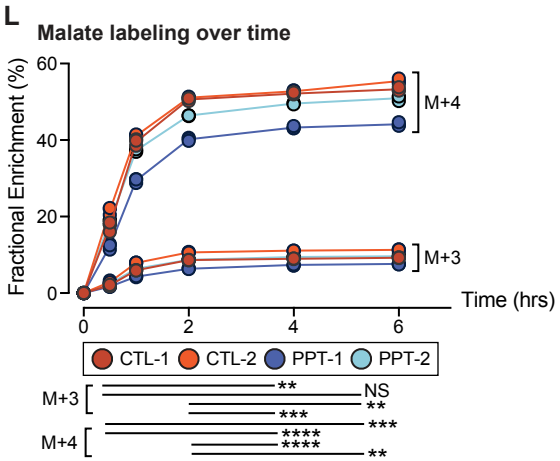

FIGURE 2: AASDHPPT is required for mtFAS

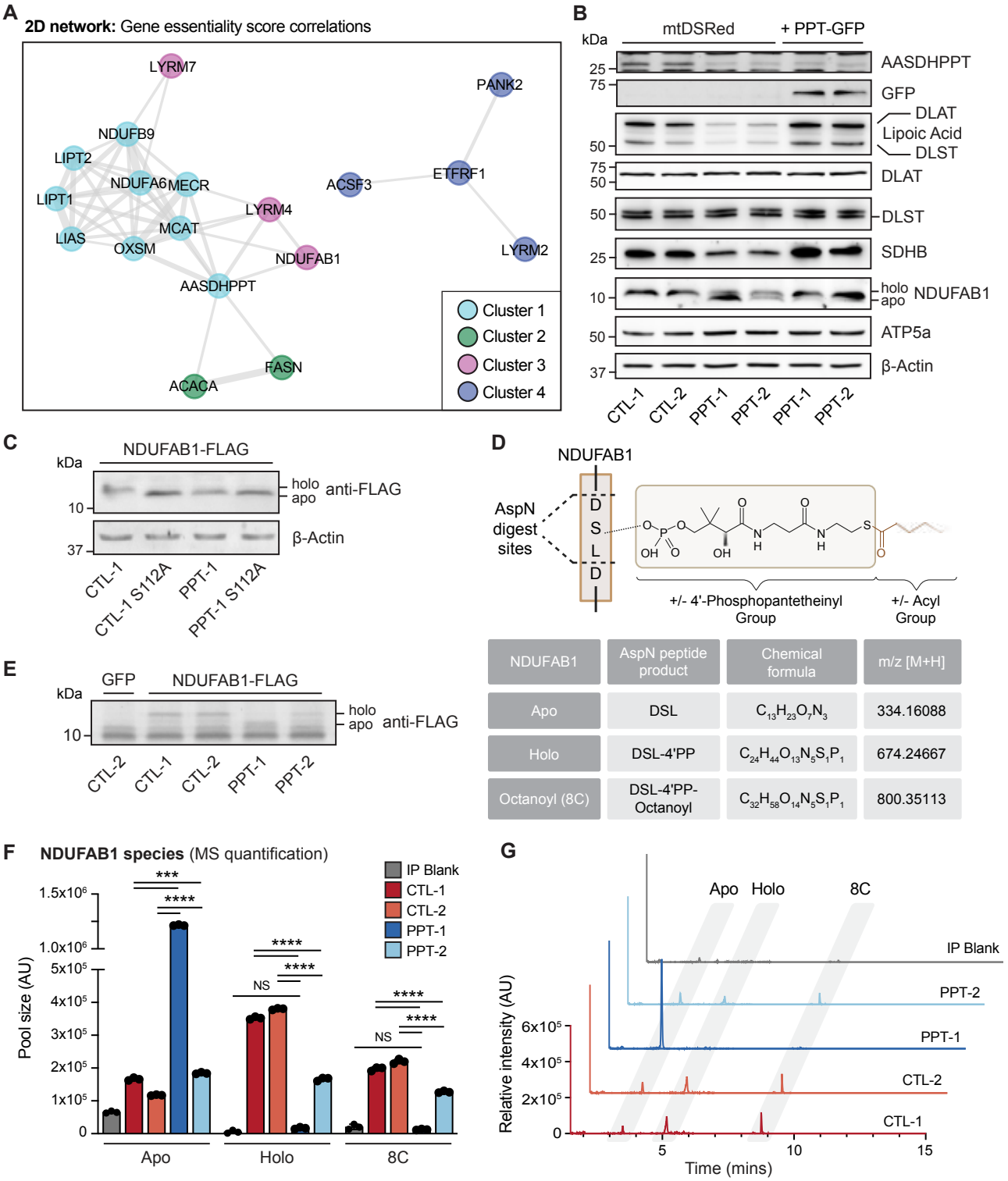

NDUFAB1	AspN peptide product	Chemical formula	m/z [M+H]
Apo	DSL	$C_{13}H_{23}O_7N_3$	334.16088
Holo	DSL-4'PP	$C_{24}H_{44}O_{13}N_5S_1P_1$	674.24667
Octanoyl (8C)	DSL-4'PP-Octanoyl	$C_{32}H_{58}O_{14}N_5S_1P_1$	800.35113

EXTENDED DATA FIGURE 2: AASDHPPT is required for mtFAS

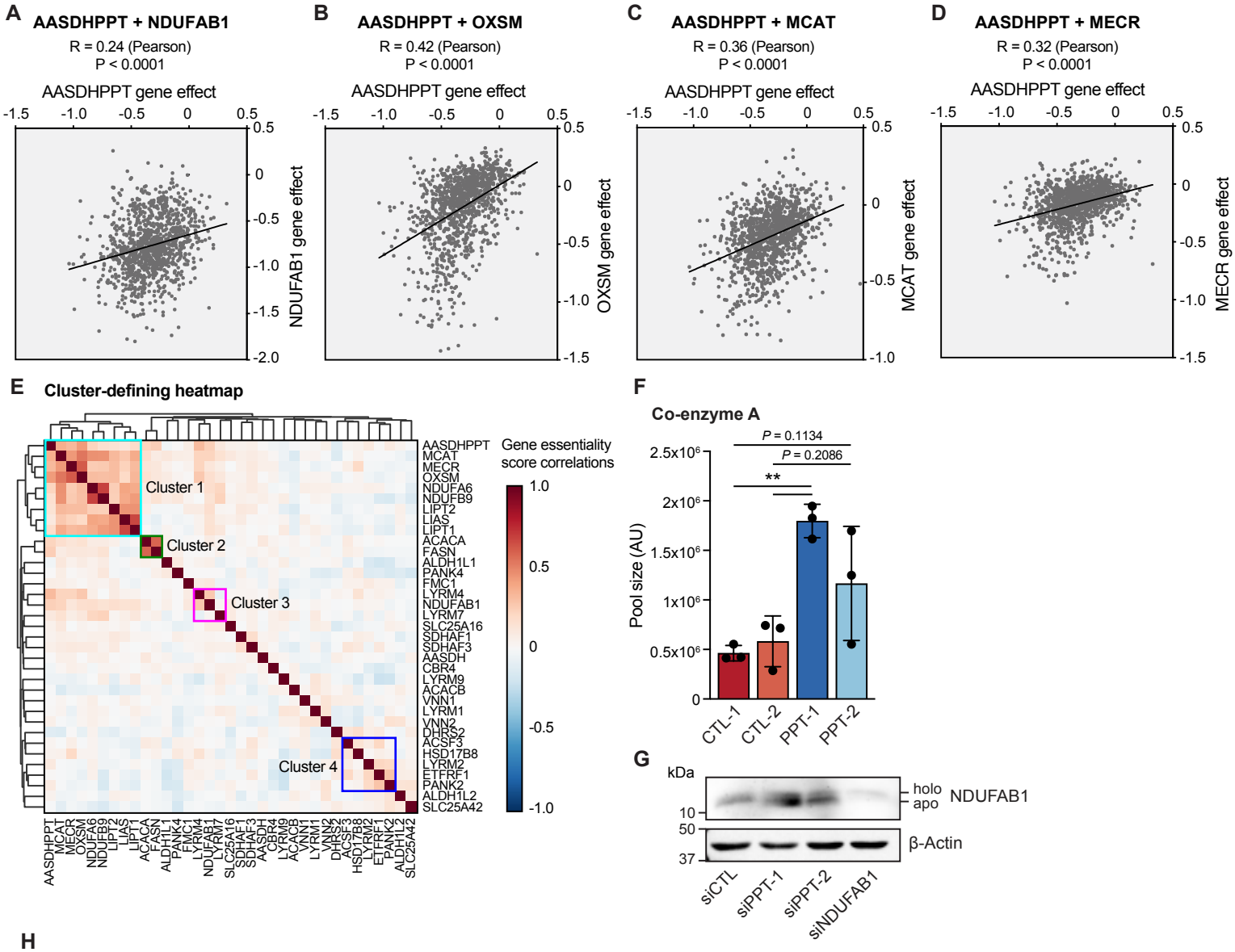

FIGURE 3: AASDHPPT localizes to the mitochondrial matrix

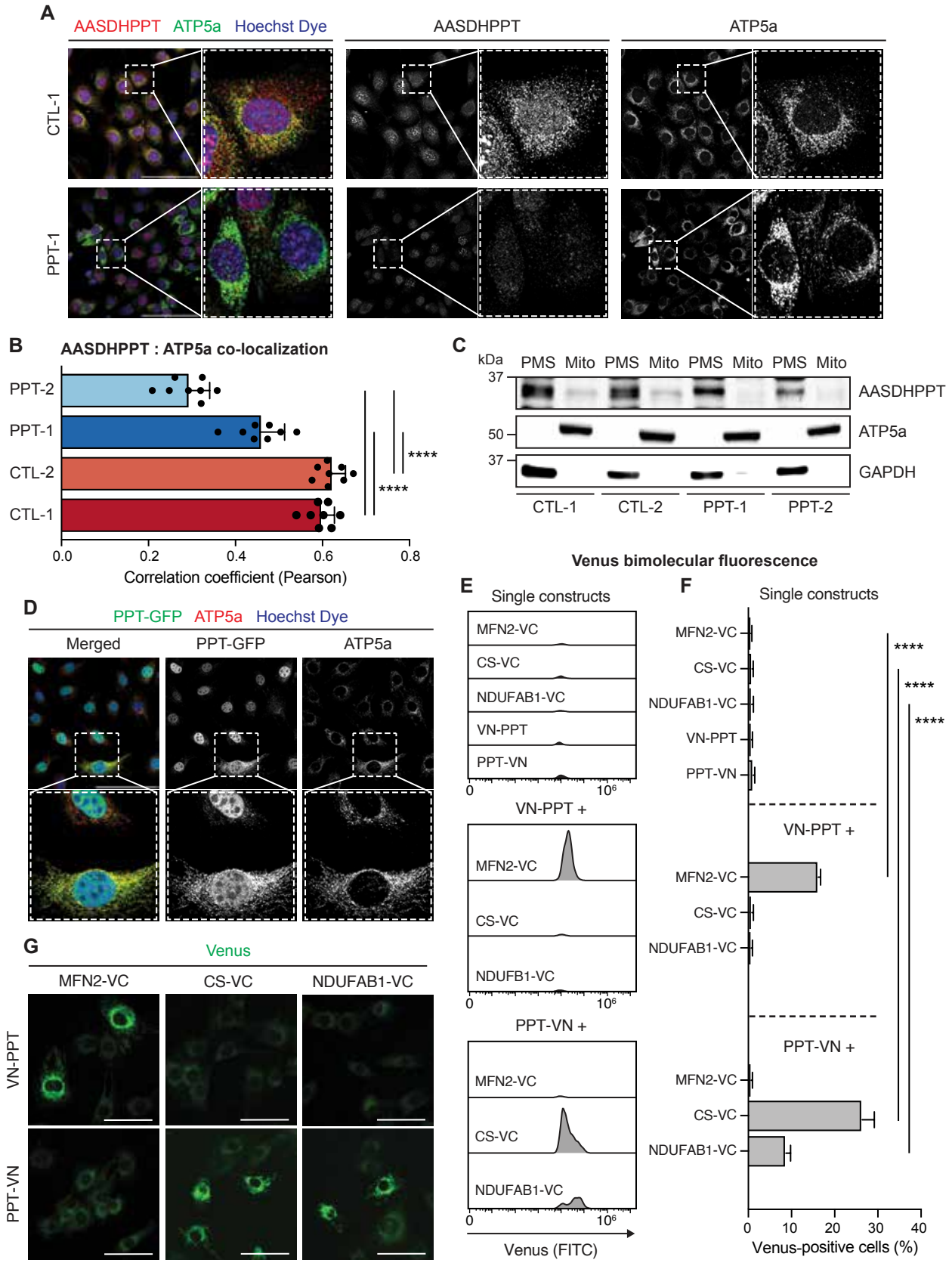

EXTENDED DATA FIGURE 3: AASDHPPT localizes to the mitochondrial matrix

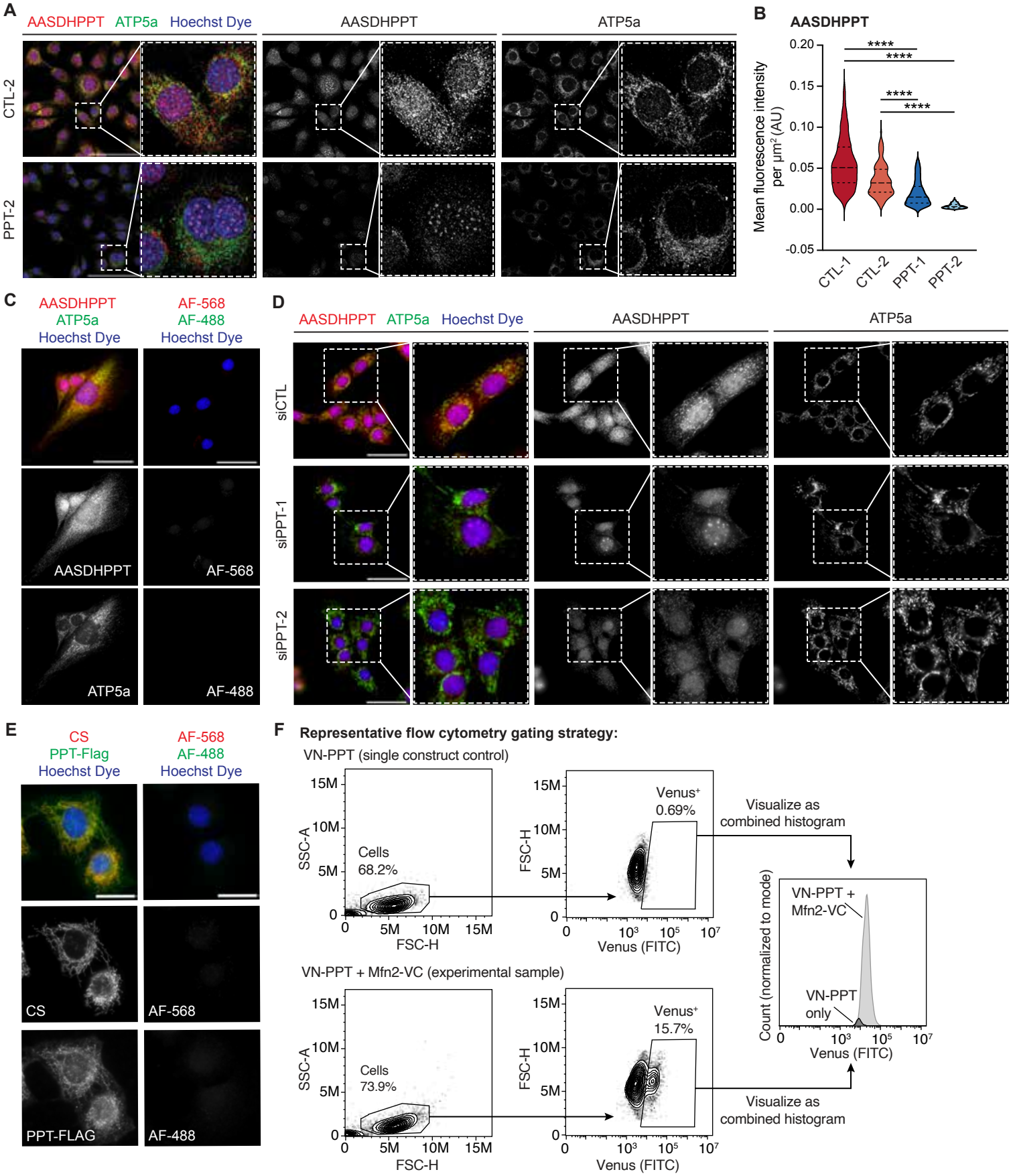

FIGURE 4: AASDHPPT has an N-terminal MTS

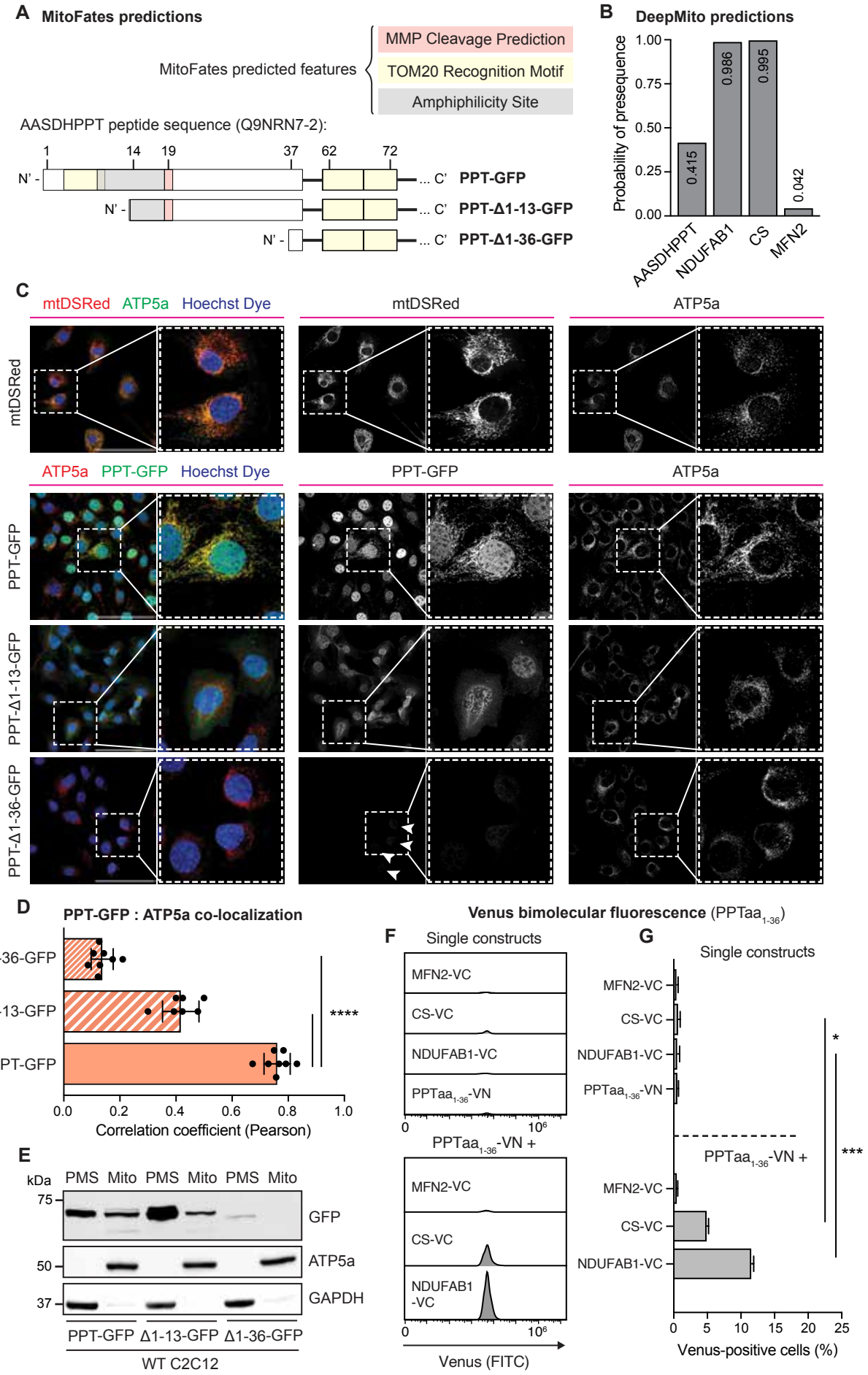

EXTENDED DATA FIGURE 4: AASDHPPT has an N-terminal MTS

A

AASDHPPT peptide sequence conservation

Species	1 … 12 14 … 37 … 47 … 72 … 79 83 … 96
Mus musculus	MVFPAKRLCVVPSMEGVRWAFSCGTWLPSRAEWLLAMRSIQPEEKERIGKFVFARDAKAALAGRLMIRKLVAEKLNIPWDHIRLQRTSKGKPVLAKDSLN...
Homo sapiens	MVFPAKRFCLVPSMEGVRWAFSCGTWLPSRAEWLLAVRSIQPEEKERIGQFVFARDAKAAMAGRLMIRKLVAEKLNIPWNHIRLQRTAKGKPVLAKDSSN...
Rattus norvegicus	MVFPAKRLCVVPYMEGVRWAFSCGTWLPSPAEWLLAVRSIQPEEKERIGQFVFARDAKAALAGRLMIRKLVAEKLNIPWDHIRLQRTSKGKPILAKDTLN...
Danio rerio	MDGVRWAFRCGSWVPSRSEWTLAARCVQQEEKLRIGQFVFAKDAKSAMAGRLLIRKLVCEKMGFAWDGFRLQRTERGKPYLPQTSSA...
Gallus gallus	MGGVRWAFPCAAWRPRREEWLLAARLVQPEEKERIGSFVYARDAKAALAGRLLMRKLIAEKLCIPWNEIHLQRTSKGKPFLANSIFS...

THE PROTEIN SCIENCE EDUCATION PROJECT

B

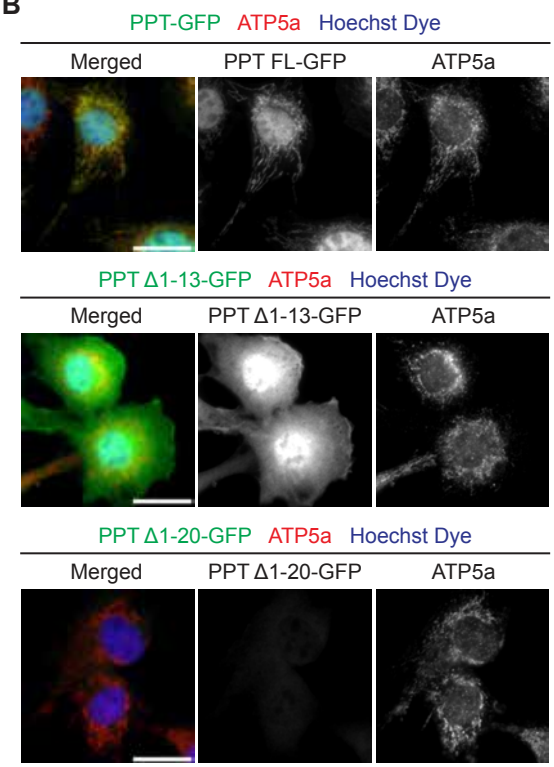

C

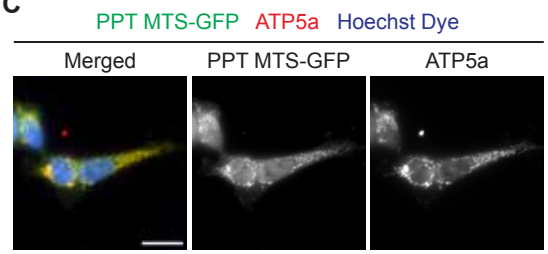

D

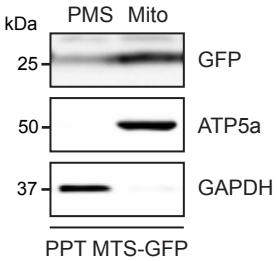

FIGURE 5: Mitochondrial localization of AASDHPPT is required for function

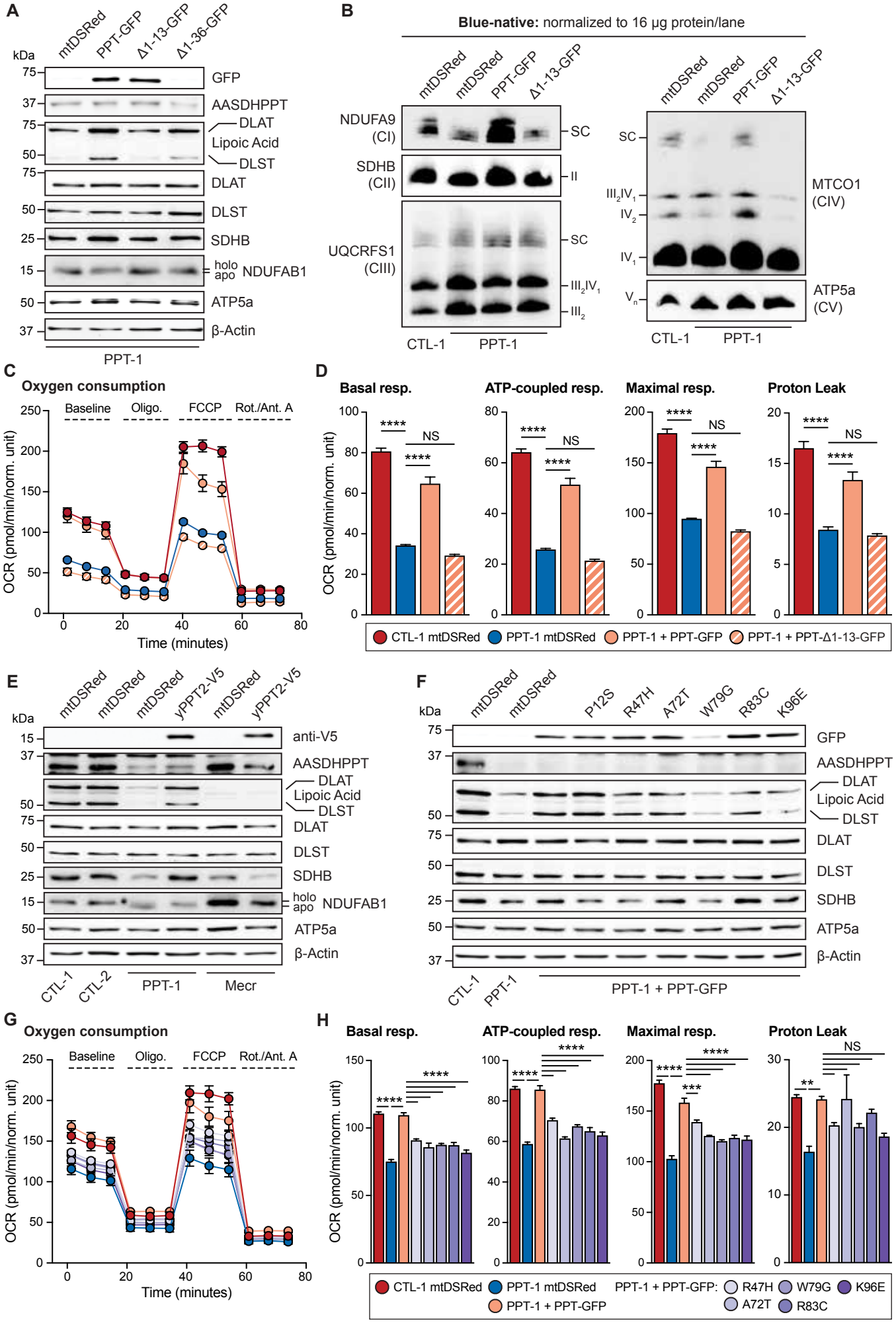
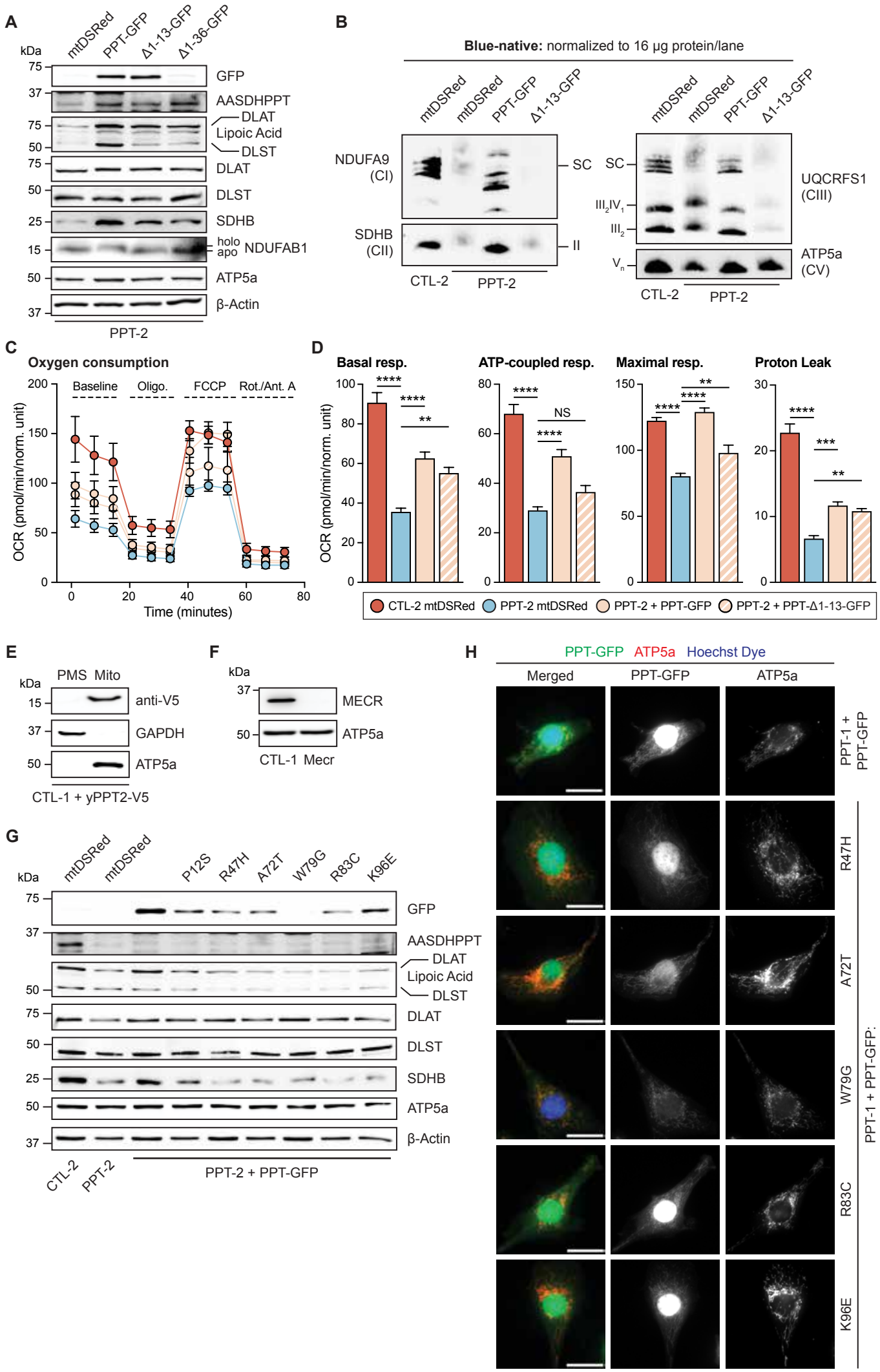
EXTENDED DATA FIGURE 5: Mitochondrial localization of AASDHPPT is required for function